

Disentangling Signatures of Selection Before and After European Colonization in Latin Americans

Javier Mendoza-Revilla  ^{1,2,3,*} J. Camilo Chacón-Duque, ^{4,5} Macarena Fuentes-Guajardo, ⁶
Louise Ormond, ¹ Ke Wang, ^{1,7} Malena Hurtado, ³ Valeria Villegas, ³ Vanessa Granja, ³
Victor Acuña-Alonso, ⁸ Claudia Jaramillo, ⁹ William Arias, ⁹ Rodrigo Barquera, ^{7,8}
Jorge Gómez-Valdés, ⁸ Hugo Villamil-Ramírez, ^{10,11} Caio C. Silva de Cerqueira, ¹² Keyla M. Badillo
Rivera, ¹³ María A. Nieves-Colón, ¹⁴ Christopher R. Gignoux, ¹⁵ Genevieve L. Wojcik, ¹⁶
Andrés Moreno-Estrada, ¹⁷ Tábita Hünemeier , ^{12,18} Virginia Ramallo, ^{12,19} Lavinia Schuler-Faccini, ¹²
Rolando González-José, ¹⁹ María-Cátira Bortolini, ¹² Samuel Canizales-Quinteros, ^{10,11} Carla Gallo, ³
Giovanni Poletti, ³ Gabriel Bedoya, ⁹ Francisco Rothhammer, ²⁰ David Balding, ^{1,21} Matteo Fumagalli , ²²
Kaustubh Adhikari, ²³ Andrés Ruiz-Linares, ^{1,24,25,*} and Garrett Hellenthal 

¹Department of Genetics, Evolution and Environment, and UCL Genetics Institute, University College London, London, United Kingdom

²Human Evolutionary Genetics Unit, Institut Pasteur, UMR2000, CNRS, Paris, France

³Laboratorios de Investigación y Desarrollo, Facultad de Ciencias y Filosofía, Universidad Peruana Cayetano Heredia, Lima, Perú

⁴Centre for Palaeogenetics, Stockholm, Sweden

⁵Department of Archaeology and Classical Studies, Stockholm University, Stockholm, Sweden

⁶Departamento de Tecnología Médica, Facultad de Ciencias de la Salud, Universidad de Tarapacá, Arica, Chile

⁷Department of Archaeogenetics, Max Planck Institute for Evolutionary Anthropology, Leipzig, Germany

⁸National School of Anthropology and History, Mexico City, Mexico

⁹GENMOL (Genética Molecular), Universidad de Antioquia, Medellín, Colombia

¹⁰Unidad de Genómica de Poblaciones Aplicada a la Salud, Facultad de Química, UNAM-Instituto Nacional de Medicina Genómica, Mexico City, Mexico

¹¹Universidad Nacional Autónoma de México e Instituto Nacional de Medicina Genómica, Mexico City, Mexico

¹²Departamento de Genética, Universidade Federal do Rio Grande do Sul, Porto Alegre, Brazil

¹³Department of Genetics, Stanford School of Medicine, Stanford, CA, USA

¹⁴Department of Anthropology, University of Minnesota Twin Cities, Minneapolis, MN, USA

¹⁵Department of Biostatistics and Informatics, University of Colorado Anschutz Medical Campus, Aurora, CO, USA

¹⁶Bloomberg School of Public Health, John Hopkins University, Baltimore, MD, USA

¹⁷Laboratorio Nacional de Genómica para la Biodiversidad (UGA-LANGEBIO), CINVESTAV, Irapuato, Guanajuato, Mexico

¹⁸Department of Genetics and Evolutionary Biology, University of São Paulo, São Paulo, Brazil

¹⁹Instituto Patagónico de Ciencias Sociales y Humanas-Centro Nacional Patagónico, CONICET, Puerto Madryn, Argentina

²⁰Instituto de Alta Investigación, Universidad de Tarapacá, Arica, Chile

²¹Schools of BioSciences and Mathematics & Statistics, University of Melbourne, Melbourne, Australia

²²School of Biological and Behavioural Sciences, Queen Mary University of London, London, United Kingdom

²³School of Mathematics and Statistics, Faculty of Science, Technology, Engineering and Mathematics, The Open University, Milton Keynes, United Kingdom

²⁴Ministry of Education Key Laboratory of Contemporary Anthropology and Collaborative Innovation Center of Genetics and Development, Fudan University, Shanghai, China

²⁵Aix-Marseille Université, CNRS, EFS, ADES, Marseille, France

***Corresponding authors:** E-mails: javier.mendoza@upch.pe; andresruiz@fudan.edu.cn; g.hellenthal@ucl.ac.uk.

[†]These authors jointly supervised this work.

Associate editor: Yuseob Kim

Abstract

Throughout human evolutionary history, large-scale migrations have led to intermixing (i.e., admixture) between previously separated human groups. Although classical and recent work have shown that studying admixture can yield novel historical insights, the extent to which this process contributed to adaptation remains underexplored. Here, we introduce a novel statistical model, specific to admixed populations, that identifies loci under selection while determining whether the selection likely occurred post-admixture or prior to admixture in one of the ancestral source populations. Through extensive simulations, we show that this method is able to detect selection, even in recently formed admixed populations, and to accurately differentiate between selection occurring in the ancestral or admixed population. We apply this method to genome-wide SNP data of ~4,000 individuals in five admixed Latin American cohorts from Brazil, Chile, Colombia, Mexico, and Peru. Our approach replicates previous reports of selection in the human leukocyte antigen region that are consistent with selection post-admixture. We also report novel signals of selection in genomic regions spanning 47 genes, reinforcing many of these signals with an alternative, commonly used local-ancestry-inference approach. These signals include several genes involved in immunity, which may reflect responses to endemic pathogens of the Americas and to the challenge of infectious disease brought by European contact. In addition, some of the strongest signals inferred to be under selection in the Native American ancestral groups of modern Latin Americans overlap with genes implicated in energy metabolism phenotypes, plausibly reflecting adaptations to novel dietary sources available in the Americas.

Key words: natural selection, Latin Americans, Native Americans, admixture.

Introduction

Admixed populations offer a unique opportunity to detect recent selection. In the human lineage, genomic studies have demonstrated the pervasiveness of admixture events in the history of the vast majority of human populations (Patterson et al. 2012; Hellenthal et al. 2014; Lazaridis et al. 2014). By inferring the ancestral origins of particular genetic loci in the genomes of recently admixed individuals, recent studies have provided evidence that such admixture has facilitated the spread of adaptative genetic mutations in humans. Notable examples include the transfer of a protective allele in the Duffy blood group gene likely providing resistance to *Plasmodium vivax* malaria in Malagasy and Cape Verdeans from sub-Saharan Africans (Hodgson et al. 2014; Pierron et al. 2018; Hamid et al. 2021), and the transmission of the lactase persistence allele in the Fula pastoralists from Western Eurasians (Vicente et al. 2019).

An ideal setting in which to test whether and how admixture contributed to genetic adaptation is Latin America. The genetic make-up of present-day Latin Americans stems mainly from three ancestral populations: indigenous Native Americans, Europeans (mainly from the Iberian Peninsula), and sub-Saharan Africans (Wang et al. 2007; Moreno-Estrada et al. 2013, 2014; Homburger et al. 2015; Chacon-Duque et al. 2018; Luisi et al. 2020) that were brought together starting ~500 years ago. The admixed genomes of Latin Americans are, thus, the result of an intermixing process between human populations that had been evolving independently for tens-of-thousands of years and that were suddenly brought together in a new environment. In this new environment, the ancestral genomes were quickly subjected to novel pressures that were largely unfamiliar from where they first evolved. Therefore, the genomes of Latin Americans

potentially harbor signals of recent adaptations attributable to beneficial variants, for example, introduced from a particular ancestral population, increasing rapidly in frequency post-admixture. Motivated by this, several studies have explored the genomes of admixed Latin Americans for signatures of selection occurring since the admixture event (Tang et al. 2007; Basu et al. 2008; Ettinger et al. 2009; Guan 2014; Rishishwar et al. 2015; Deng et al. 2016; Zhou et al. 2016; Norris et al. 2020; Vicuna et al. 2020). These studies have relied on an approach similar to that of admixture mapping, where the ancestry of a genomic region in each admixed individual is assigned to a particular ancestral population, a technique known as local-ancestry-inference (LAI). Loci with significantly more inferred ancestry inherited from one ancestral population are assumed to have evolved under some form of selection (Tang et al. 2007).

In addition, the genetic makeup of Latin Americans offers the opportunity to detect selection in their ancestral populations, as large cohorts of Latin Americans can be leveraged to reconstruct genetic variation patterns in each source population. This is of particular use for exploring selection in Native Americans, since Native American groups are currently underrepresented in genomic studies (Sirugo et al. 2019), and as a consequence, only a few studies have centered on detecting adaptive signals of indigenous groups from the Americas. Such studies have identified strong selective signals at different genes, particularly at those related to immunity, highlighting the selective pressures that Native Americans were subjected to after they entered the continent (Lindo et al. 2018; Reynolds et al. 2019; Avila-Arcos et al. 2020).

With some exceptions (Cheng et al. 2021), these studies either limited their analyses to Latin Americans with high Native American ancestry or used LAI to infer loci in

individuals that derive from a Native American source. However, such approaches may result in a reduction of statistical power due to the removal of individuals with non-Native American ancestry, inaccurate local ancestry estimation, and/or through removing segments challenging to assign.

Here, we present a novel statistical model that identifies loci that have undergone selection before or after an admixture event (which we refer to as pre- or post-admixture selection, respectively). In contrast to previous methods, this approach is based on allele frequencies and does not require assignments of local ancestry along the genome. We illustrate the utility of our new method by performing a selection scan in five Latin American cohorts collected as part from the CANDELA Consortium (Ruiz-Linares et al. 2014). Our results suggest that several loci have been subjected to natural selection in admixed Latin American populations, and in their ancestral populations, replicating many of these signals using LAI. Many of the putative selected single nucleotide polymorphisms (SNPs) are strongly associated to relevant phenotypes, or act as expression quantitative loci (eQTL) in relevant tissues, providing further evidence of their functional effect. Overall, our analyses highlight the usefulness of our method to detect signals of selection in

admixed populations or their ancestral populations, and reveal novel candidate genes implicated in the adaptive history of groups from the American continent.

Results

Overview of AdaptMix

In part following Balding and Nichols (1995), and analogous to previous approaches (Long 1991; Mathieson et al. 2015; Cheng et al. 2021), our model AdaptMix assumes that, under neutrality, the allele frequencies of an admixed target population can be described using a beta-binomial model, with expected allele frequency equal to a mixture of sampled allele frequencies from a set of groups that act as surrogates to the admixing sources (fig. 1). In our case, the admixed target population is a Latin American cohort, defined below, and we use three surrogate groups to represent Native American, European, and African admixing source populations. The mixture values are inferred a priori, for example, using ADMIXTURE (Alexander et al. 2009) (fig. 1A), qpAdm (Haak et al. 2015) or SOURCEFIND (Chacon-Duque et al. 2018), as the average amount of ancestry that each admixed target individual matches to a set of reference populations.

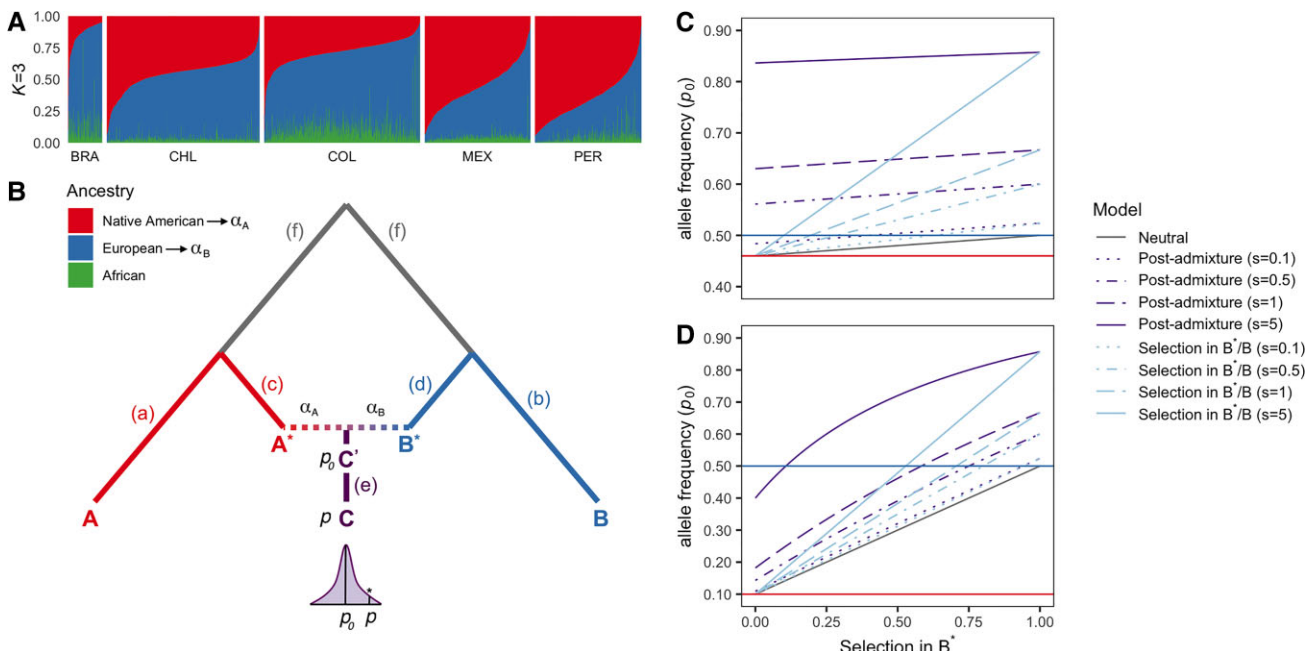


Fig. 1. Schematic and intuition of the AdaptMix model. (A) For each CANDELA individual (columns), ADMIXTURE-inferred proportions of ancestry related to Native American, European, and African reference individuals. (B) Assuming only two admixing sources in this illustration for simplicity, the model assumes ancestral populations (A^* and B^*) contribute ancestry proportions α_A and α_B , respectively, to an admixed population (C) that is ancestral to the tested population (C'). Assuming neutrality, the expected allele frequency (p_0) of C is estimated using these proportions and the allele frequencies surrogate populations A and B related to A^* and B^* , respectively. The sampled allele frequency (p) of C is compared with p_0 , with large deviations indicative of selection (shown with an asterisk in the distribution). (c and d) The relationship between p_0 , the expected allele frequency in the admixed population under neutrality or selection, and α_B , the ancestry proportion contributed from ancestral population B^* . If selection occurred prior to admixture during the split between populations B^* and its surrogate B (i.e., along the blue branch in [B]), this relationship increases linearly (blue lines), becoming more differentiated from neutrality (gray line) as the admixture from B^* increases. In contrast, under selection post-admixture (i.e., along the purple branch in [B]), the expected allele frequency (purple lines) can deviate from neutrality even when the admixture from B^* is near 0. The difference between the post-admixture and pre-admixture lines is more clear when allele frequencies in populations A and B are similar (top plot). The solid blue and red lines indicate the allele frequencies in the surrogate populations A and B , which are used to calculate p_0 .

(The reference populations used by these programs may be the same as the surrogate populations used in *AdaptMix*, but they need not be as illustrated below.) We find the variance parameter that maximizes the likelihood of this beta-binomial model across all SNPs. This variance term aims to limit the number of false-positives attributable to genetic drift in the target population following admixture and/or the use of inaccurate surrogates for the ancestral populations. Then, at each SNP, we calculate the probability of observing allele counts equal to or more extreme than those observed in the target population, hence providing a *P* value testing the null hypothesis that the SNP is neutral (see Materials and Methods).

Assuming a pulse of admixture, this test is designed to detect selection occurring: 1) in the admixed population following the admixture event (i.e., along the purple line “e” in *fig. 1B*), and/or 2) in one (or more) of the source/surrogate pairings (i.e., along the red and/or blue lines (a)–(d) in *fig. 1B*). Note that scenario 2) includes selection occurring in any of the ancestral source populations (i.e., along the lines “c” or “d” in *fig. 1B*) and/or in any of the surrogate populations (i.e., along the lines “a” or “b” in *fig. 1B*). At SNPs with evidence of selection (i.e., low *P* values), we distinguish between 1) and 2) by exploring how genotype counts of admixed target individuals relate to their inferred admixture proportions contributed by each surrogate. Under scenario 1), we assume that selection affects all target individuals equally, regardless of their admixture proportions, which, in turn, assumes that all ancestries were present when selection occurred. In contrast, under scenario 2), we expect selection to more strongly affect one of the source/surrogate population pairings. Intuitively, if 2) is true, individuals with nearly 100% ancestry from the source/surrogate pair experiencing selection will have genotype counts that deviate the most from expectations under the neutral model, whereas individuals with nearly 0% ancestry from this pair will have counts that closely follow the neutral model (*fig. 1C*). If instead 1) is true, this pattern is attenuated, though it can be challenging in practice to distinguish 2) from 1) if allele frequencies strongly differ between surrogate groups (*fig. 1D*). Assuming a multiplicative model of selection, which is numerically close to an additive model, we find the selection coefficients that maximize the fit of the data to model 1) and to model 2) when separately treating each source/surrogate pair as the selected group. We report ratios of likelihoods, equivalent here to using differences in Akaike Information Criterion (AIC), to quantify our ability to distinguish among scenarios 1) and 2).

In summary, for each tested SNP we infer 1) a *P* value testing the null hypothesis of neutrality, 2) the relative evidence (i.e., likelihood ratios) for whether selection occurred post-admixture or in one of the admixing sources and 3) the selection strength summed across time.

Simulations

We tested our approach using simulations designed to resemble our Latin American cohort in terms of sample size,

inferred admixture proportions, and the extent to which our surrogates match the true admixing sources. As post-admixture selection in recently admixed population is challenging to detect unless selection is strong, we included selection coefficients (*s*) of large magnitude. We note that the upper range values are consistent with those estimated in recently admixed populations, including Latin Americans (Zhou et al. 2016, Pierron et al. 2018, Vicente et al. 2019, Hamid et al. 2021) (see Materials and Methods).

At a false-positive rate of 5×10^{-5} , these simulations indicate we have ~ 50 –90% power to detect selection for scenario 1) (i.e., post-admixture selection) with $s = 0.15$ –0.20, with *s* defined as the selection strength per generation in homozygotes carrying two copies of the selected allele, and selection occurring over 12 generations under various modes of selection (additive, dominant, multiplicative, recessive) (*fig. 2A*, *supplementary fig. S1*, *Supplementary Material* online). For scenario 2), in the case of selection occurring in the Native American source, power depends on the overall amount of Native American ancestry (*fig. 2A*). As an example, Brazil-like simulations (<15% average Native American ancestry) show little power, Colombia-like simulations ($\sim 30\%$ average Native American ancestry) typically exhibit >50% power, and other simulated populations (~ 50 –70% average Native American ancestry) exhibit >75% power under scenario 2) assuming $s \geq 0.1$ over 50 generations, with similar power if instead $s \sim 0.025$ over 150 generations (*supplementary fig. S2*, *Supplementary Material* online). Simulations including a bottleneck in the Native American source population (see Materials and Methods) showed reduced power, likely because the stronger genetic drift both masks the selection signal (Refoyo-Martínez et al. 2019; Cuadros-Espinoza et al. 2021) and makes the surrogate population more genetically differentiated from its corresponding source (*supplementary fig. S3*, *Supplementary Material* online). Detecting selection occurring in the European or African source depends on the overall amount of European and African ancestry in a similar manner (e.g., *fig. 2A*, *supplementary figs. S4* and *S5*, *Supplementary Material* online). For SNPs where we detect selection, we mis-classify the type of selection $\leq 2\%$ of the time, for example, concluding post-admixture selection when the truth is selection in the Native American source $\sim 1\%$ of the time across all selection coefficients (*fig. 2B*). However, our approach often fails to classify selection scenarios unless selection strengths are large (e.g., $s > 0.1$).

We also compared the power of *AdaptMix* to that of *Ohana*, a recently developed maximum likelihood method that infers selection by modeling ancestral admixture components, which has been shown to have similar or higher power to other state-of-the-art methods (Cheng et al. 2021). Following Cheng et al. (2021), we simulated a realistic demographic model relating four populations meant to represent African, East Asian, European, and Native American sources. We also simulated an admixed population that descends from a 50 to 50% mixture of the European and Native American sources, with selection

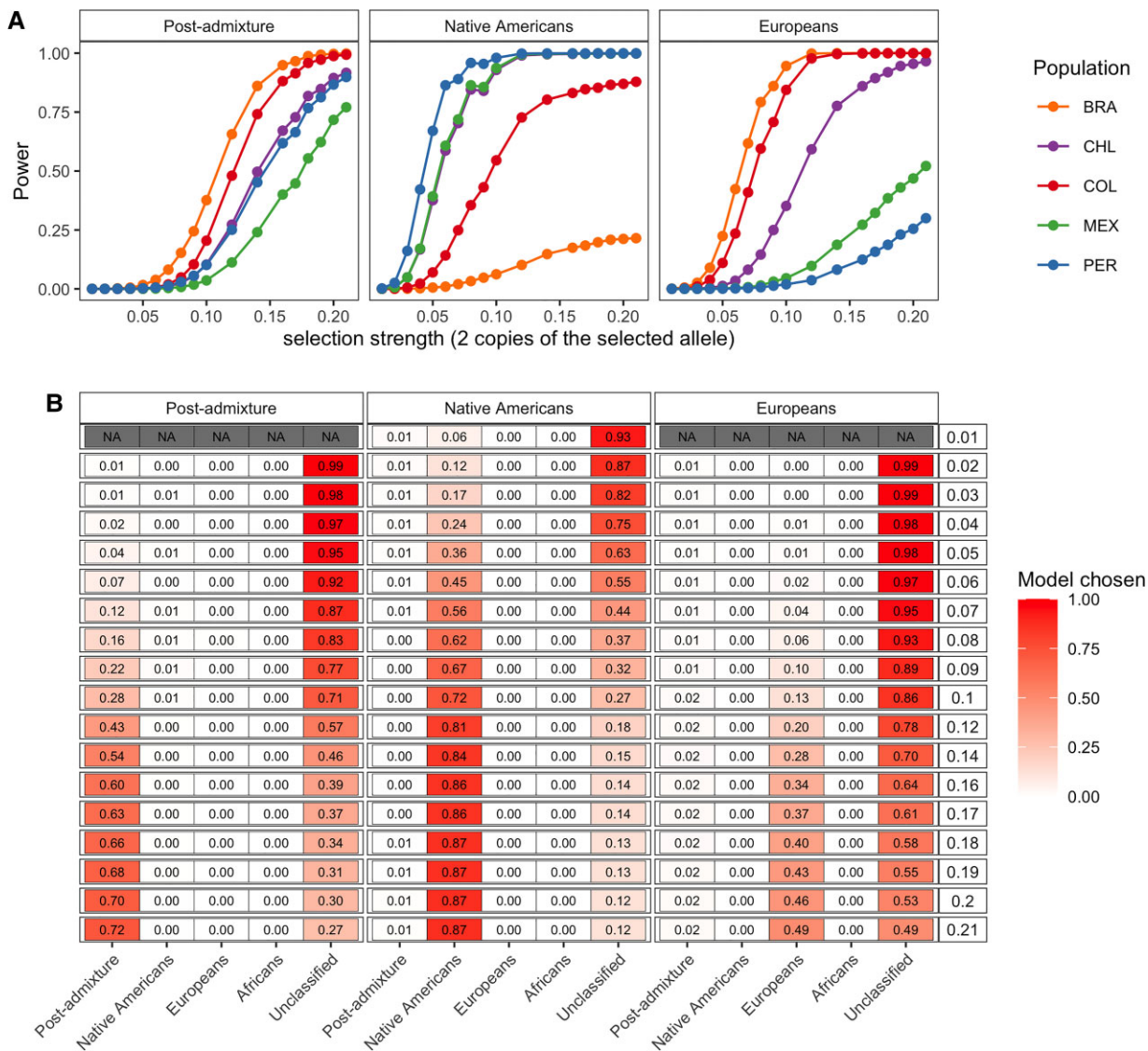


Fig. 2. Performance of AdaptMix to detect and classify selection in simulated Latin American populations. (A) Power to detect selection post-admixture, selection in Native Americans, or selection in Europeans in simulated populations mimicking the Latin American cohorts. Power is based on a P value cutoff that resulted in a false-positive rate of 5×10^{-5} in neutral simulations. The power estimated for a given selection coefficient is based on combining simulations using four different modes of selection (additive, dominant, multiplicative, recessive) occurring over 12 generations for the post-admixture simulations, over 50 generations for the selection in Native American simulations, and over 25 generations for the selection in European simulations. Each simulation for a given combination of parameters consisted of 10,000 advantageous SNPs with a starting allele frequency of the advantageous allele lower than 0.5. (B) The proportion of significant SNPs from (A) that were assigned to the correct simulated scenario of (left-to-right) post-admixture selection or selection in Native Americans or Europeans (using a likelihood ratio $>1,000$ to make a call; otherwise “Unclassified”). Rows give the true selection coefficient (legend at right), and the heatmap values give the classification rate. Rows with N.A. show instances with less than 50 selected SNPs for which the classification rate is poorly estimated.

occurring prior to admixture in only the ancestral Native American source (see Materials and Methods). We then applied AdaptMix and Ohana to four sampled populations that descend from the Africa, East Asian, European, and admixed populations. In these simulations, AdaptMix has $\sim 0.4\text{--}4.8\%$ less power than Ohana if running Ohana with an ideal number of ancestry components K , in this case $K = 4$, that distinguishes the admixed population (supplementary fig. S6, Supplementary Material online), and if Ohana only tests for selection in the ancestry component most representative of the admixed population (fig. 3A). However, AdaptMix has up to 5.12% more power

than Ohana in this setting when using Ohana’s more general test that does not assume selection only in the admixed population. Furthermore, if using a suboptimal K , for example, $K = 3$, Ohana’s power is greatly reduced, since the Native American and East Asian sources are both classified into the same ancestry component (supplementary fig. S6, Supplementary Material online). We also performed simulations, mimicking those in Cuadros-Espinoza et al. (2021), under which selection occurs post-admixture in the admixed population, with admixture occurring 70 generations ago (see Materials and Methods). In these simulations, AdaptMix outperformed Ohana even when using

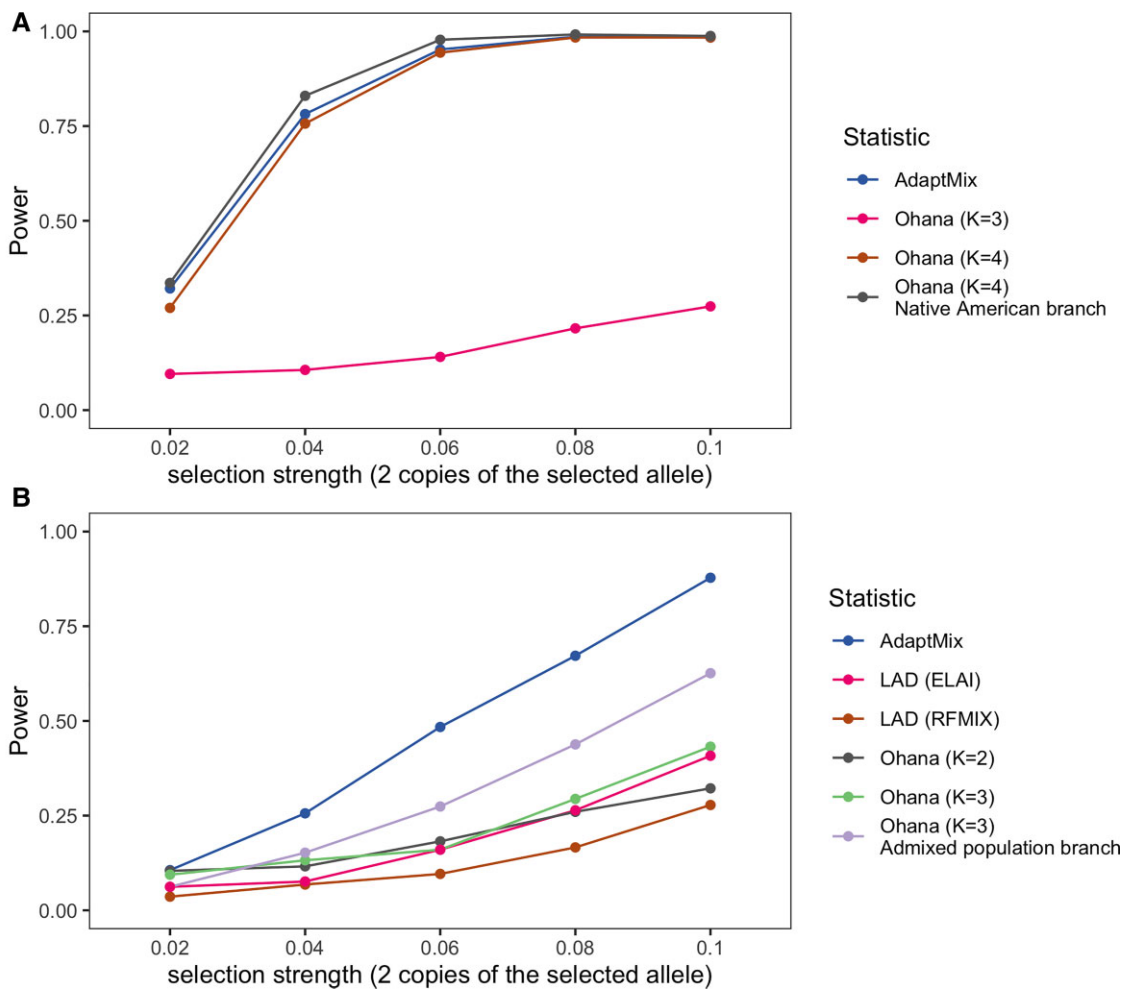


Fig. 3. Performance of AdaptMix compared with existing methods. (A) Power of AdaptMix and Ohana to detect selection occurring prior to admixture only in the Native American source of an admixed population. The gray line depicts Ohana's power with $K = 4$ when testing for selection only in the ancestry component most representative of the Native American source, with the brown line testing under the general model. (B) Power of AdaptMix, Ohana, and two LAD approaches (RFMix, ELAI; [Maples et al 2013](#), [Guan 2014](#)) to detect selection occurring in an admixed population directly following the admixture event. The purple line depicts Ohana's power with $K = 3$ when testing for selection only in the ancestry component most representative of the admixed population, with the green line testing under the general model. See Methods section for a detailed explanation of the simulation parameters employed for each scenario. Power for (A) and (B) is based on a P value cutoff that resulted in a false-positive rate of 0.05 in neutral simulations.

the ideal number of clusters $K = 3$, presumably because Ohana does not classify the admixed individuals into their own ancestry component ([supplementary fig. S6, Supplementary Material online](#)), which should maximize its power. In these post-admixture simulations, both AdaptMix and Ohana outperform two local ancestry deviation (LAD) approaches (RFMix, ELAI) ([Maples et al. 2013](#); [Guan 2014](#)), perhaps because the older admixture time resulted in difficulties accurately assigning local ancestry segments to source populations.

Applying AdaptMix to the Five Latin American Cohorts of CANDELA

We divided Latin Americans into five cohorts based on country of origin: Brazil ($n = 190$), Chile ($n = 896$), Colombia ($n = 1,125$), Mexico ($n = 773$), and Peru ($n = 834$), using individuals sampled as part of the CANDELA

Consortium ([Ruiz-Linares et al. 2014](#)), testing each cohort for selection separately ([supplementary fig. S7, Supplementary Material online](#)). Analyzing each cohort by country of origin results in a higher number of individuals, and, thus, increases the statistical power to detect selection. As demonstrated in [Chacon-Duque et al \(2018\)](#), however, there is a notable population sub-structure within each country. To test for robustness of our selection signals to this sub-structure, we supplemented each of these analyses by testing subsets of individuals within a country based on their inferred ancestry matching to Native American reference groups from [Chacon-Duque et al. \(2018\)](#). This gave six additional tested groups with sufficient ancestry represented: “Mapuche” ($n = 434$) in Chile, “Chibcha Paez” ($n = 200$) in Colombia, “Nahua” ($n = 466$) and “South Mexico” ($n = 78$) in Mexico, and “Andes Piedmont” ($n = 195$) and “Quechua” ($n = 147$) in Peru ([supplementary fig. S8, Supplementary Material](#)

online). To infer the proportion of African, European, and Native American ancestry in each Latin American, we applied unsupervised ADMIXTURE with $K = 3$ clusters jointly to all CANDELA individuals and 553 Native American, Iberian, and West African reference individuals (fig. 1A).

Note that the choice of surrogate populations defines the selection test between each surrogate and its corresponding ancestral source in scenario 2). In this way, our test acts as an analogue to F_{ST} comparing two populations, but while accounting for admixture in one of the populations. As an illustration, we tested the Brazilian cohort for selection using northwest Europeans from England and Scotland (GBR) from the 1000 Genomes Project (1KGP) (The 1000 Genomes Project Consortium 2015) as a surrogate for the Brazilian cohort's European ancestry source (supplementary fig. S9, Supplementary Material online). Given the majority ($\sim 80\%$) of ancestry in the Brazilian cohort is related to Iberian Europeans, this test is most-powered to detect selection acting along the branch separating present-day northwest Europeans and descendants of Iberians who traveled to Brazil post-Columbus. In this analysis, we infer the strongest signals of selection at the *HERC2/OCA2* and *LCT/MCM6* genes. This replicates previously reported selection signals when comparing northwest Europeans to present-day Iberians (Poulter et al. 2003; Bersaglieri et al. 2004) and likely indicates selection for lighter skin pigmentation and lactase persistence in northwest Europeans that is unrelated to any selection in the Americas.

As another example, we also tested each Latin American cohort separately while using Han Chinese from Beijing (CHB) from the 1KGP as a surrogate for Native American ancestry (supplementary fig. S10, Supplementary Material online). In this analysis, SNPs that follow model 2) indicate selection along the branch separating present-day Han Chinese and Native American populations. For this test, we find the strongest signals of selection at previously reported selected genes in East Asians, including those related to alcohol metabolism such as *ADH7* and *ADH1B* (Galinsky et al. 2016; Gu et al. 2018) that are both classified as selection under model 2). The strongest overall signal in this scan, which was unclassified, overlapped the *POU2F3* gene, implicated in the regulation of viral transcription, keratinocyte differentiation, and other cellular events. Selection signals at this gene have been reported to be under selection in Native American populations from throughout the Americas (Amorim et al. 2017) and also shows evidence for Neanderthal adaptive introgression in East Asians (Racimo, Marnetto, et al. 2017).

For our main analyses, we use 205 Iberians (from 1KGP and Chacon-Duque et al. (2018)) to represent European ancestry surrogates. Therefore, given the likely short split time between present-day Iberians and Europeans who migrated to the Americas during the colonial era, we are underpowered to detect selection in the European source only (see simulations). We use 206 West Africans from the 1KGP to represent the African ancestry source, which has been reported as a good proxy to the African genetic

sources (from Chacon-Duque et al. (2018)). For this reason, we should similarly have low power to find selection occurring only in the African source/surrogate. At any rate we do not test for selection related to African ancestry, because the Latin American cohort here have $\sim 6\%$ African ancestry on average, limiting power further (see supplementary fig. S5, Supplementary Material online). We combined 142 individuals with $<1\%$ non-Native American inferred ancestry from 19 Native American groups (supplementary table S1, Supplementary Material online) to represent the Native American surrogate. By using individuals sampled from geographically spread Native American groups as the Native American ancestry surrogate, we aim to identify regional selection signals experienced by some Native American groups but not others. We also expect to have the highest power when testing for selection type 2) in Native Americans, as there is likely to be the most time separating this "average" Native American surrogate and the admixing source of each regional Latin American cohort. To avoid confounding our inference, we excluded individuals with $>1\%$ inferred ancestry matching to surrogates other than Native Americans, Iberian Europeans, and West Africans using SOURCEFIND (Chacon-Duque et al. 2018). Also, since the time since admixture among these groups is relatively short in the CANDELA cohort (likely <15 generations ago), detecting selection post-admixture can only identify relatively strong selection signals (see simulations).

AdaptMix Identifies 47 Regions of Putative Selection

For each Latin American cohort, we considered SNPs under selection as those having P values less than the 5×10^{-5} false-positive threshold in the population-matched neutral simulations, which corresponds to a model-based P value of 6.75×10^{-6} – 1.07×10^{-7} (supplementary table S2, Supplementary Material online). For Chile, Colombia, Mexico, and Peru, we report loci that pass these criteria both in the analysis of all individuals from that country and in at least one of three alternative analyses for that country that are designed to test for robustness to latent population structure (supplementary fig. S11, Supplementary Material online). The first of these alternative analyses consisted of identifying signals of selection using AdaptMix on each of the six Native American subsets defined above (e.g., in either the "Andes Piedmont" or "Quechua" subset when testing for selection in Peruvians) (supplementary table S3, Supplementary Material online). The other two alternative analyses were based on LAI. In particular, we used ELAI (Guan 2014) to assign each genomic region of an admixed individual to a Native American, European, or African ancestral source. For the second alternative analysis, designed to test for post-admixture selection, we assessed whether the proportion of ancestry inferred from one of these three sources in a local region deviated substantially from the genome-wide average (supplementary table S4, Supplementary Material online). For the third alternative analysis, designed to test for

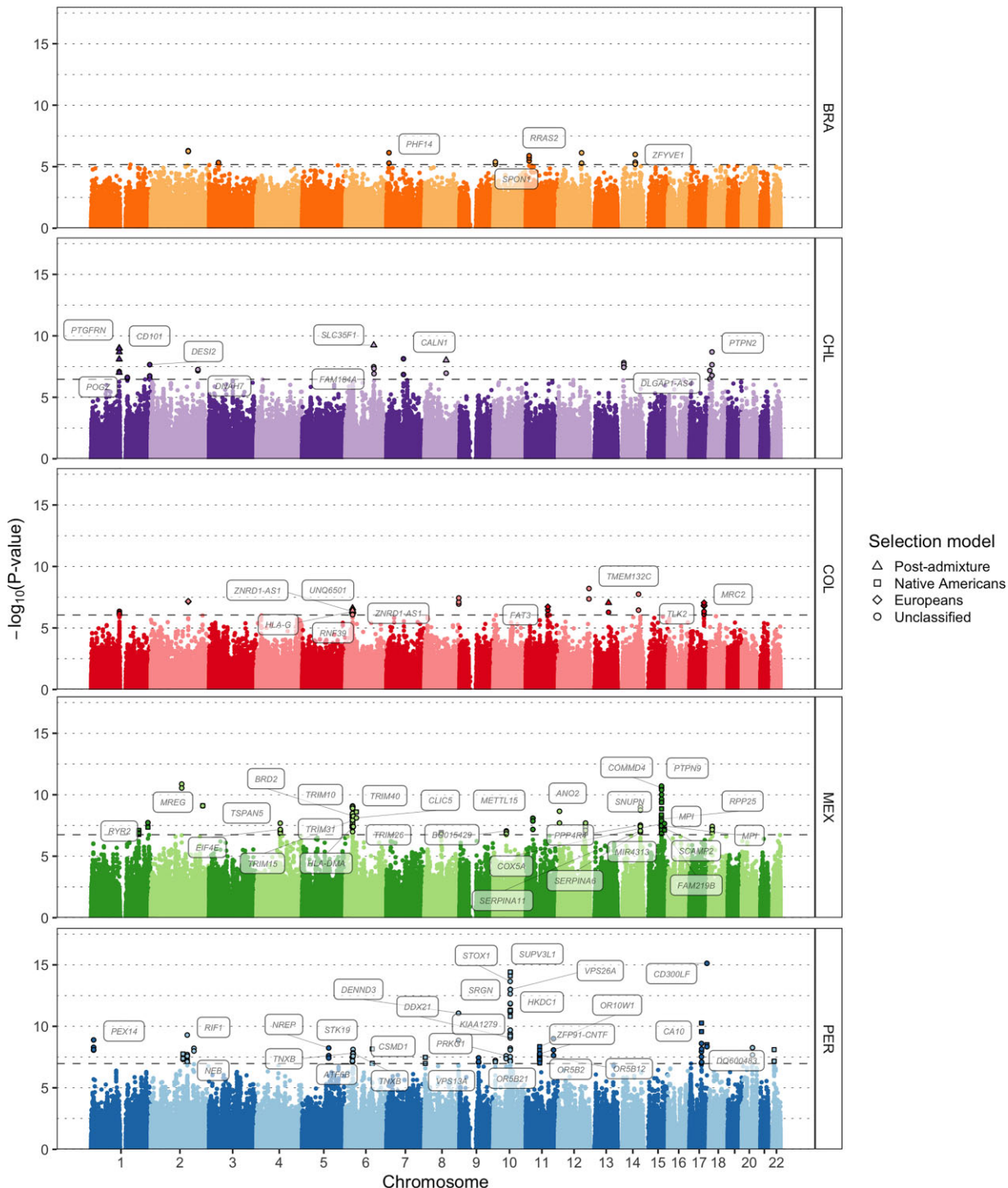


Fig. 4. Genome-wide selection scan in five Latin American cohorts. Manhattan plot showing the genomic regions identified as selected via AdaptMix in each Latin American cohort. The dashed horizontal lines indicate the P values cutoffs corresponding to a false-positive rate of 5×10^{-5} based on neutral simulations. Different shapes represent the most likely selection model. The names of genes associated with significant SNPs are shown.

selection in the Native American source, we instead used the Population Branch Statistic (PBS) (Yi et al. 2010) to test for selection in one of the six Native American subset groups defined above, using allele frequencies computed from LAI-inferred Native American segments from the subset of individuals representing that Native American group (see Materials and Methods) (supplementary fig. S8,

Supplementary Material online and supplementary table S5, Supplementary Material online).

Overall, we find 51 candidate regions to have evidence of positive or purifying selection passing the criteria above, 47 of which target protein-coding genes (supplementary table S6, Supplementary Material online and fig. 4). Four of these 47 candidate gene regions contain at least one

SNP exhibiting strong evidence (likelihood ratio $>1,000$) of selection affecting all admixed individuals regardless of ancestry proportions, which we assume reflects post-admixture selection. Furthermore, 18 of these 47 regions exhibit strong evidence of selection containing at least one SNP (likelihood ratio $>1,000$) in the Native American source only. The 25 remaining candidate gene regions are unclassified into either type of selection (likelihood ratio $\leq 1,000$).

To prioritize candidate causal genes, we annotated the protein-coding gene that had the highest overall Variant-to-Gene (V2G) scores (Ghousaini et al. 2021; Ochoa et al. 2021) for the SNPs showing the strongest evidence of selection in each candidate gene region. The overall V2G score aggregates differentially weighted evidence of variant-gene association from several sources, including cis-QTL data, chromatin interaction experiments, in silico function predictions (e.g., Variant Effect Predictor from Ensembl), and distance between the variant and each gene's canonical transcription starting site. For each of these candidate genes, we then annotated the phenotype with the highest overall association score based on the Open Targets Platform (Koscielny et al. 2017; Ochoa et al. 2021).

Although most of these associated phenotypes represent genetic disorders, syndromes, or different types of measurements (medically or non-medically related), many are also related to immune response and diet—two major selective forces previously reported to shape the human genome (Karlsson et al. 2014; Fan et al. 2016). We, therefore, organize the description of our candidate selection signals into two main sections below that cover only these two features, with signals of all other hits in [supplementary table S6, Supplementary Material online](#). For brevity, below we only highlight putatively selected regions where at least one significant SNP had an associated GWAS or eQTL signal. For our significant SNPs related to immune-response genes, GWAS signals included SNPs associated to white blood cell counts in a large multicontinental cohort (including Latin American individuals) (Chen et al. 2020), and eQTL signals included cis-associated SNPs to gene expression in 15 immune-related cell types from the DICE project (Schmiedel et al. 2018). For our significant SNPs related to diet, GWAS signals included metabolic, anthropometric, and lipid levels from the UK Biobank cohort (Loh et al. 2018), and eQTL signals included cis-associated SNPs to gene expression in adipose, muscle, and liver tissue from the GTEx Project (Lonsdale et al. 2013).

Signals at Immune-Related Genes

Fifteen of the forty-seven candidate gene regions contained at least one protein-coding gene either related to the development or regulation of the immune system or that has been previously associated to the quantification of immune cell types, susceptibility progression to infectious diseases, or autoimmune disorders. For example, we replicate a well-known signal encompassing several immune-related genes

at 6p21 that are a part of the human leukocyte antigen (HLA) system ([fig. 4](#) and [supplementary figs. S12–S14, Supplementary Material online](#)). These included SNPs (AdaptMix P value $< 5.00 \times 10^{-7}$) near several MHC class I genes (*HLA-G*, *HLA-H*, *HLA-A*, and *HLA-J*) in each of the Chilean, Colombian, Mexican, and Peruvian cohorts, with the Colombian cohort containing several SNPs classified as being selected post-admixture (likelihood ratio $>1,000$). Encouragingly, we inferred African ancestry enrichment (Z -score > 2.5) in each cohort ~ 60 kb downstream from our top AdaptMix signals using LAI, with maximum Z -score > 9 (one-sided P value $< 4.09 \times 10^{-21}$) in the Chilean cohort ([fig. 5](#)). In addition, other signals were inferred upstream in the Chilean cohort at a 5' UTR SNP of the *ZBTB12* gene (rs2844455, AdaptMix P value $= 5.45 \times 10^{-8}$), the Mexican cohort at an intronic SNP of *HLA-DMA* (rs28724903, AdaptMix P value $= 3.87 \times 10^{-8}$), and the Peruvian cohort at an intronic SNP of the MHC class III gene *STK19* (rs6941112, AdaptMix P value $= 7.57 \times 10^{-9}$). Many of these HLA genes have been previously characterized as subject to be under selection post-admixture in different Latin American populations by showing an excess of African ancestry at the HLA locus (Tang et al. 2007; Basu et al. 2008; Ettinger et al. 2009; Guan 2014; Rishishwar et al. 2015; Deng et al. 2016; Zhou et al. 2016; Norris et al. 2020; Vicuna et al. 2020).

In addition to HLA, we infer previously unreported selection signals in four candidate gene regions that each harbor genes with well-established roles in the immune system, with each region containing at least one SNP significantly associated (P value $< 5 \times 10^{-8}$) to white blood cell counts or the expression of an immune-related gene in immune cells (P value $< 10^{-5}$) (see Materials and Methods). Among these, one signal at 1p13 in the Chilean cohort encompasses the *CD101* gene ([fig. 6A](#)), which belongs to a family of cell-surface immunoglobulins superfamily proteins and plays a role as an inhibitor of T-cell proliferation (Soares et al. 1998; Bouloc et al. 2000). Within this region, five SNPs are classified as being selected post-admixture and also show an increase of LAI-inferred European ancestry (maximum Z -score $= 3.40$, one-sided P value $= 3.36 \times 10^{-4}$). Strikingly, the region contains a synonymous SNP (Ile588, CADD score of 9.23) (rs3736907, AdaptMix P value $= 1.05 \times 10^{-9}$) that strongly affects *CD101* expression in T cells (eQTL P value $< 2.42 \times 10^{-10}$) and is associated with neutrophil (GWAS P value $= 2.08 \times 10^{-10}$) and total white cell count (GWAS P value $= 3.61 \times 10^{-9}$) ([fig. 6A](#)).

The second signal, at 18p11 also in Chileans, encompasses the *PTPN2* gene, a tyrosine-specific phosphatase involved in the Janus kinase (JAK)-signal transducer and activator of transcription (STAT) signaling pathway ([fig. 6B](#)). The JAK-STAT pathway has an important role in the control of immune responses, and dysregulation of this pathway is associated with various immune disorders (Shuai and Liu 2003). Several SNPs with low AdaptMix P values (P value $< 1.69 \times 10^{-7}$) in the 18p11 region are also associated with eosinophil counts (GWAS P value $<$

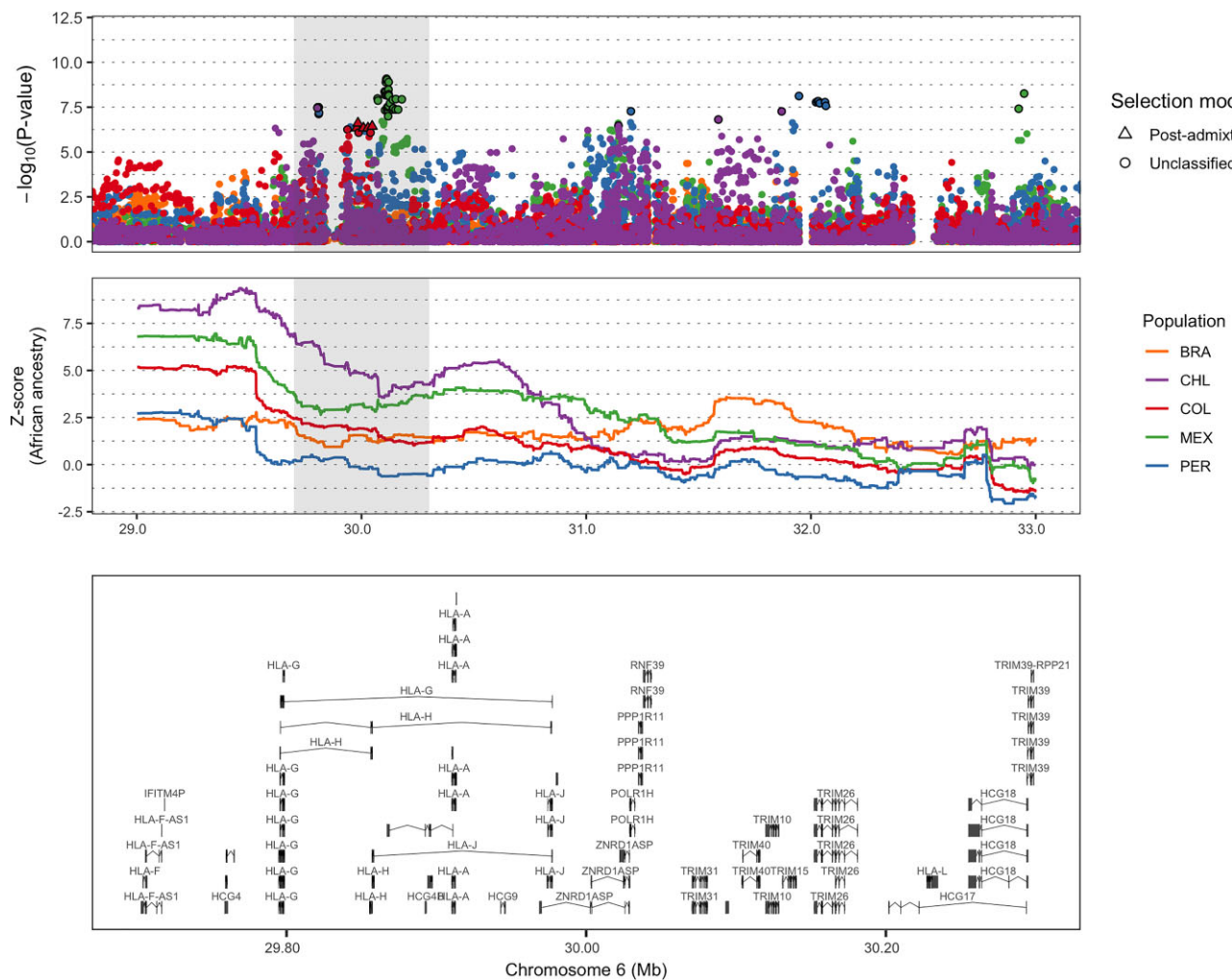


Fig. 5. Regional selection plot at the HLA region in five Latin American cohorts. The top plot shows the $-\log_{10}(P\text{ value})$ of SNPs from AdaptMix, the middle plot shows Z-score values based on African LADs, and the bottom plot shows genes in the region shaded in gray. Genomic coordinates are in Mb (build hg19 as reference) and genes shown include transcripts.

1.13×10^{-10}) and the expression of *PTPN2* in natural killer (NK) cells (eQTL P value $< 1.14 \times 10^{-9}$) (fig. 6B).

The other two novel signals, both in the Peruvian cohort, are consistent with selection in Native Americans only (likelihood-ratio $> 1,000$). The first, at 17q25, contains the *CD300LF* gene that encodes for a membrane glycoprotein that contains an immunoglobulin domain, and that plays an important role in the maintenance of immune homeostasis by promoting macrophage-mediated efferocytosis (Borrego 2013). Notably, a 3'UTR SNP (rs9913698, AdaptMix P value $= 3.11 \times 10^{-9}$) is strongly associated with monocyte count (GWAS P value $= 1.00 \times 10^{-33}$), total white cell count (GWAS P value $= 5.96 \times 10^{-24}$), lymphocyte count (GWAS P value $= 2.50 \times 10^{-19}$), and neutrophil count (GWAS P value $= 1.30 \times 10^{-9}$) (supplementary fig. S15, Supplementary Material online). The second signal is at 22q11 adjacent to the *MIF* gene (fig. 6C), which is implicated in macrophage function in host defense through the suppression of anti-inflammatory effects of glucocorticoids (Calandra and Roger 2003). Variants within *MIF* have been recently

associated to rheumatoid arthritis in southern Mexican patients (Santoscoy-Ascencio et al. 2020). The SNP rs2330635 (AdaptMix P value $= 7.06 \times 10^{-8}$) is strongly associated to the expression of *MIF* in T-cells (eQTL P value $< 8.63 \times 10^{-5}$) and NK cells (eQTL P value $= 5.77 \times 10^{-9}$) and is also marginally associated to neutrophil counts (GWAS P value $= 2.46 \times 10^{-6}$) (fig. 6C).

Overall, these findings suggest that some of the clearest signals of adaptation in the Americas can be ascribed to immune-related selective pressures. These plausibly resulted from both the introduction of novel pathogens after European colonization and the endemic pathogens encountered by the first Native Americans during the initial peopling of the continent.

Signals at Genes Related to Diet

Among the 47 candidate regions, nine regions contained at least one protein-coding gene potentially related to dietary practices through their association with metabolism-related phenotypes or anthropometric-related

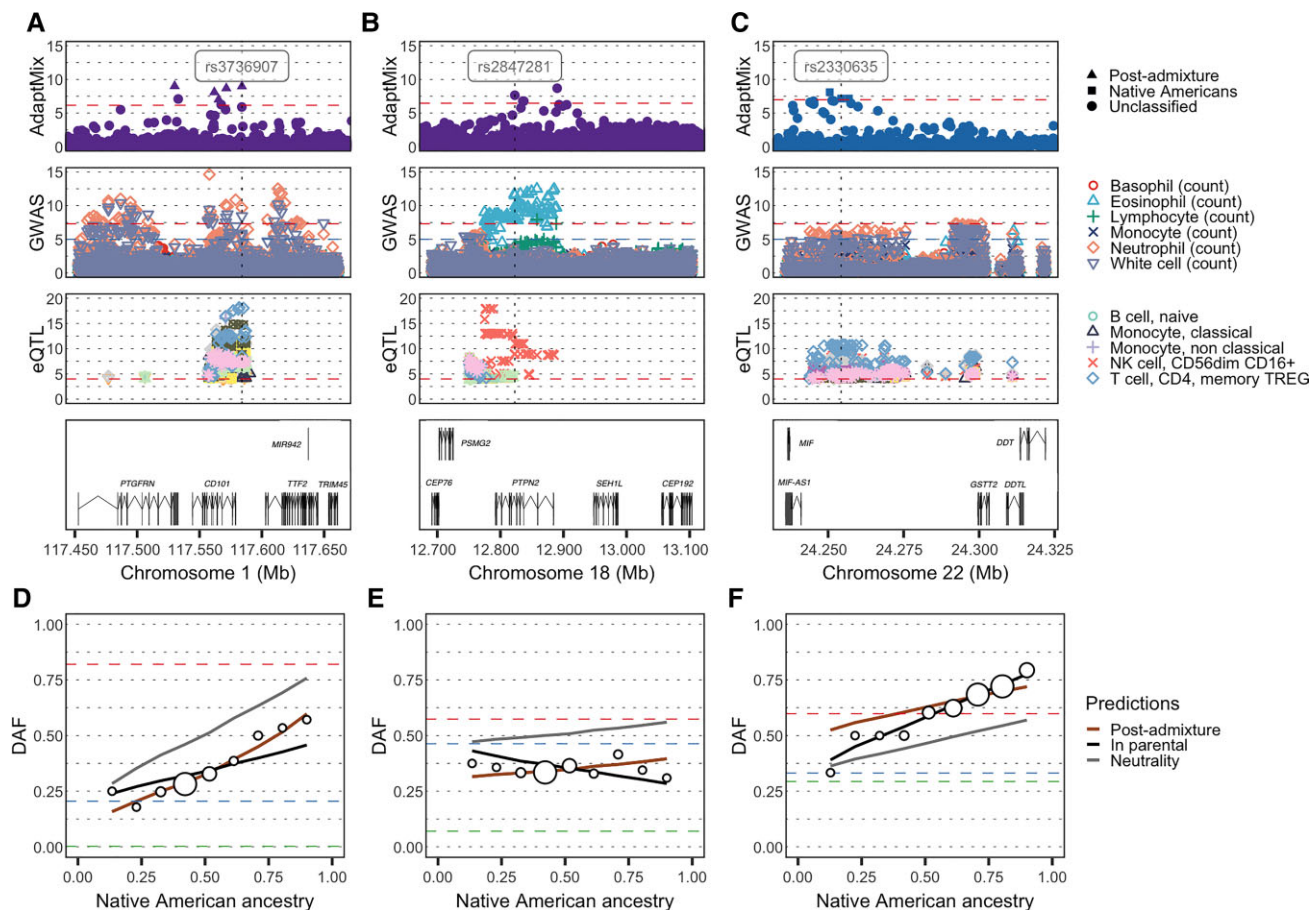


Fig. 6. Genetic loci with signals of selection at immune-related genes. (A), (B) and (C) Regional selection plot at three candidate regions of selection encompassing two immune-related genes in the Chilean and one immune-related gene in the Peruvian cohort. Each plot is composed of four panels (rows), consisting of $-\log_{10}(P)$ values of SNPs: (row 1) from AdaptMix; (row 2) associated with immune-related cell counts via GWAS (Chen et al 2020); (row 3) associated (as expression quantitative trait loci [eQTLs]) with expression of genes *CD101*, *PTPN2*, and *MIF* for (A)–(C), respectively (Schmiedel et al. 2018); with (row 4) depicting genes in the region (in Mb, build hg19 as reference). The horizontal dashed lines give significance thresholds of (row 1) P value $= 1 \times 10^{-5}$ based on neutral simulations (row 2) P value $= 1 \times 10^{-5}$ (blue line) and P value $= 5 \times 10^{-8}$ (red line), and (row 3) P value $= 1 \times 10^{-4}$. (D), (E) and (F) Derived allele frequency (DAF) in admixed Latin Americans (white circles) stratified by proportion of inferred Native American ancestry, for the SNPs highlighted (vertical dashed line) in top row panels. The sizes of the circles are proportional to the number of individuals in that particular bin. The lines give expected DAF under neutrality (gray), post-admixture selection (brown), or selection in the Native source (black). The horizontal dashed red, blue, and green lines depict DAF for surrogates to Native American, European, and African sources, respectively. AdaptMix's conclusions for these SNPs are selection that is (D) post-admixture, (E) unclassified, and (F) pre-admixture in the Native American source.

measurements (supplementary table S6, Supplementary Material online). Among these, we infer three previously unreported signals where at least one of the selected SNPs was associated to metabolic- or anthropometric-related phenotypes, or to the expression of the candidate gene in adipose, muscle, or liver tissue (see Materials and Methods). One of these three hits (rs4636058, AdaptMix P value $= 5.70 \times 10^{-10}$), at 6p22 in the Chilean cohort, is classified as being selected post-admixture and shows an increase of LAI-inferred European ancestry (Z -score $= 3.78$, one-sided P value $= 7.82 \times 10^{-4}$). It is located at 6q22 and encompasses the *SLC35F1* gene, whose function is not known, though several studies have associated this gene with different measurements of cardiac function (Hoffmann et al. 2017; Warren et al. 2017; Giri et al. 2019). Notably, SNP rs4636058 is marginally associated to cholesterol levels

(UKBB GWAS P value $= 3.8 \times 10^{-4}$) and body fat percentage (UKBB GWAS P value $= 4.29 \times 10^{-4}$). Another of these three hits, at 1q31 in the Mexican cohort, is consistent with selection in Native Americans (likelihood-ratio $> 1,000$) (fig. 7A). The 1q31 signal includes an intronic SNP (rs1171148, AdaptMix P value $= 2.31 \times 10^{-8}$) of *BRINP3*, a gene associated to body mass index in studies across different human groups (Pulit et al. 2019; Zhu et al. 2020). Within this region, various SNPs are associated to different metabolic-related phenotypes, including the SNP rs1171148 that is associated with hip circumference (UKBB GWAS P value $= 4.96 \times 10^{-8}$) and marginally associated with the body mass index (UKBB GWAS P value $= 5.51 \times 10^{-5}$) (fig. 7A).

Finally, the third hit (rs5030938, AdaptMix P value $= 3.79 \times 10^{-15}$), which had the highest overall AdaptMix score, is inferred in the Peruvian cohort at 10q22 and

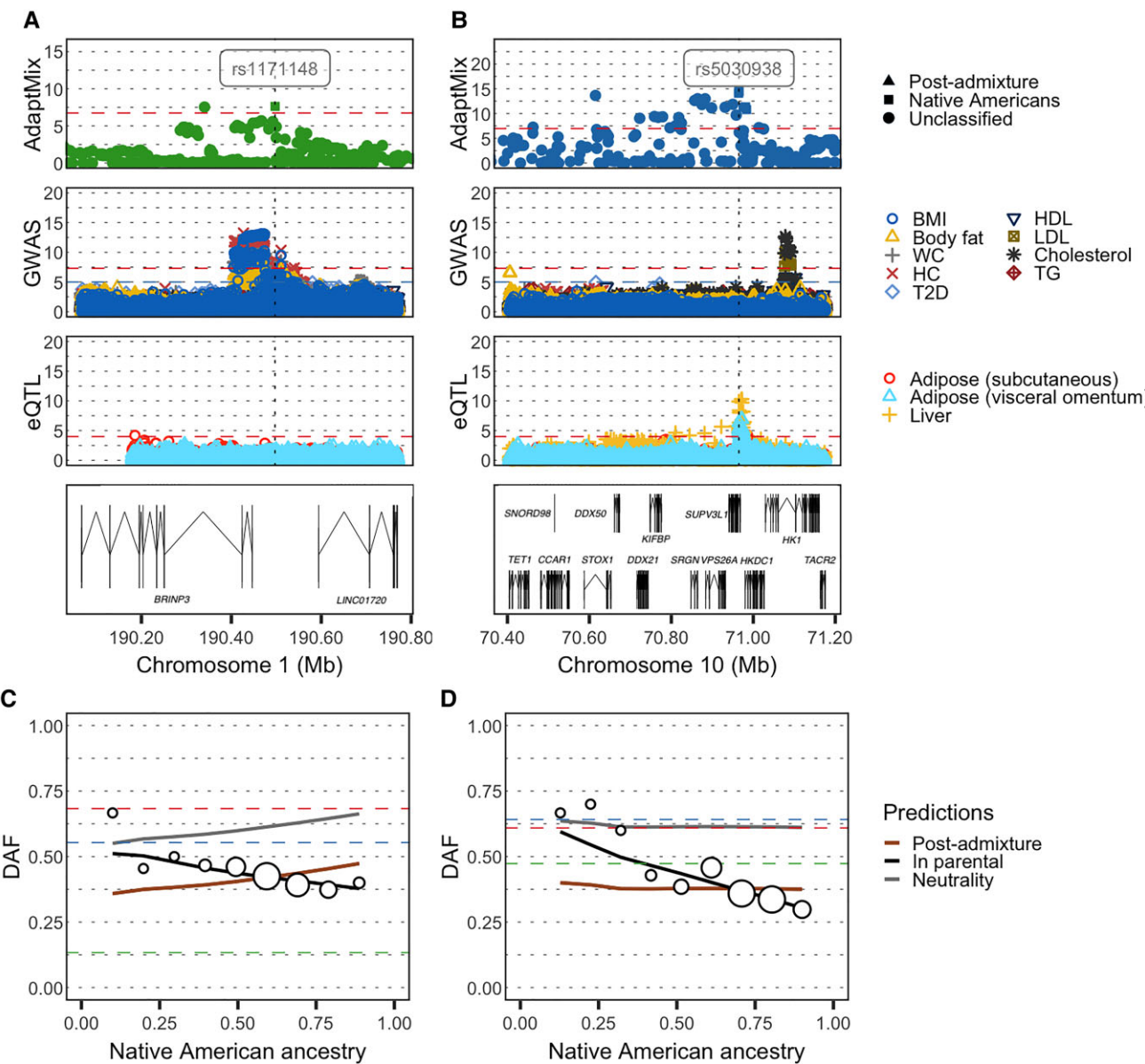


Fig. 7. Genetic loci with signals of selection at metabolic-related genes. (A) and (B) Regional selection plot at two candidate regions of selection encompassing metabolic-related genes in the Mexican and Peruvian cohorts, respectively. Each plot is composed of four panels consisting of $-\log_{10}(P$ values) of SNPs: (row 1) from AdaptMix; (row 2) from the UK Biobank GWAS; (row 3) associated (as eQTLs) with expression of BRINP3 and HKDC1 for (A)–(B), respectively, (GTEx eQTL study); with (row 4) depicting genes in the region (in Mb, build hg19 as reference). The horizontal dashed lines give significance thresholds of (row 1) P value = 1×10^{-5} based on neutral simulations (row 2) P value = 1×10^{-5} (blue line) and P value = 5×10^{-8} (red line), and (row 3) P value = 1×10^{-4} . (C) and (D) Derived allele frequency (DAF) in admixed Latin Americans (white circles) stratified by the proportion of inferred Native American ancestry, for the SNPs highlighted (vertical dashed line) in top row panels, both of which were classified as reflecting selection in the Native American source. The sizes of the circles are proportional to the number of individuals in that particular bin. The lines give expected DAF under neutrality (gray), post-admixture selection (brown), or selection in the Native American source (black). The horizontal dashed red, blue, and green lines depict DAF for surrogates to Native American, European, and African sources, respectively. AdaptMix's conclusions for these SNPs are selection that is pre-admixture in the Native American source for (C) and (D).

indicates selection in Native Americans (likelihood-ratio $>1,000$) (fig. 7B). This SNP is associated with the expression of HKDC1 in liver (eQTL P value = 2.19×10^{-5}), adipose visceral (eQTL P value = 1.46×10^{-5}), and adipose subcutaneous tissue (eQTL P value = 1.36×10^{-4}) (fig. 6B). HKDC1 encodes hexokinase that catalyzes the rate-limiting and first obligatory step of glucose metabolism (Ludvik et al. 2016), and several studies have

associated variants within this gene with glucose levels in pregnant women (Hayes et al. 2013; Guo et al. 2015; Kanthimathi et al. 2016; Tan et al. 2019) and with weight at birth (Warrington et al. 2019).

Overall, these results support previous hypothesis that genes related to energy metabolism were probably critical in the establishment of stable human populations in distinct ecoregions (Hancock et al. 2010),

including those of the Americas (Amorim et al. 2017; Reynolds et al. 2019).

Discussion

Analytical Considerations

Here, we present AdaptMix, a novel statistical model that identifies loci under selection in admixed populations. Our model is based on the principle that allele frequencies in an admixed population can be modeled as a linear combination of the allele frequencies in the ancestral populations proportional to their admixing contributions, and that deviations from the expectation can be a product of selection. This selection test is related to the work of Long (1991) and Mathieson et al. (2015). One difference is that our approach directly infers and models the variance of the predicted allele frequencies in the admixed population given the set of surrogates used for ancestral sources. This parameter can help control for large deviations in allele frequency arising solely from genetic drift experienced in the admixed population (Long 1991; Bhatia et al. 2014) and/or from using inaccurate proxies for one or more of the source populations. In some applications here, for example, the Brazilian cohort, AdaptMix gives *P* values with a median near 0.5 as expected under the null hypothesis of neutrality (supplementary fig. S16, Supplementary Material online). However, simulations under neutrality that follow a slightly different model than our inference approach (see Materials and Methods), shows AdaptMix gives both an excess of high and low *P* values relative to the uniform distribution expected under neutrality (supplementary fig. S17, Supplementary Material online). This suggests our *P* values are not well-calibrated, perhaps reflecting deviations from the underlying model and necessitating caution when choosing thresholds for significance. One potential issue is that SNPs with low minor-allele-frequency (MAF) likely well-fit their expected frequencies under the neutral model, given their lower expected variance in sampling frequency. Therefore, datasets with a high proportion of such SNPs may decrease the inferred variance parameter to an undesirably low value. Binning SNPs by MAF and inferring a separate variance parameter for each bin may help. Here, we based our significance thresholds on neutral simulations tailored to each cohort, including matching for genome-wide sampled allele frequencies, and focus only on the strongest association signals that resulted in low false-positive rates based on simulated neutral SNPs. However, we caution that necessarily simulations are over-simplifications of complex latent demographic processes, and more work is required to verify these signals.

Another important contribution of our test is that it can infer whether selection disproportionately affects one source/surrogate pairing or affects all ancestry backgrounds equally. We assume that selection affecting all ancestry backgrounds indicates selection occurring post-admixture, which is more parsimonious than an

alternative explanation of independent selection events differentiating allele frequencies between each admixing source and its surrogate. For inferred selection in a source/surrogate pairing, this can reflect selection occurring in that source and/or its surrogate, possibly even following the admixture event. Post-admixture selection affecting only one source may be possible in cases of selection only occurring in a particular environment that is correlated with admixture fractions. For example, selection we infer to occur in Native Americans may be attributable to Europeans introducing a new environmental pressure (e.g., infectious disease) that disproportionately affected fitness in indigenous Americans. However, the split time between the true Native American ancestral source and our Native American surrogate is likely much longer than the time since colonial era admixture, suggesting selection pre-admixture as a more plausible explanation given the longer time to act. Supporting this, our inferred selection coefficients (which are summed over time) in cases where we conclude selection in Native Americans are typically greater than 2 (supplementary table S6, Supplementary Material online). If selection had occurred post-admixture continuously over the last 12 generations (corresponding to an admixture date of ~1650CE), this value approximately corresponds to a per generation selection coefficient ~0.16, which is strong relative to previous reports of recent selection in human populations (e.g., Hamid et al. (2021)). In contrast, our four signals concluding post-admixture selection infer a per generation selection coefficient <0.1, which falls more in line with previous inference of selection strengths.

For 18 genomic regions where we conclude selection in the Native American source (supplementary table S6, Supplementary Material online), it is possible this is capturing selection in (some subset of) groups that comprise the Native American surrogate group we use here, rather than in the (more localized) Native American source of the admixed population. The lack of overlap in selection signals when analyzing the five CANDELA cohorts, as well as the lack of concordance of our signals with those from PBS testing for selection in this combined Native American surrogate (supplementary fig. S18, Supplementary Material online), suggests that our signals are not being driven by selection in this combined population in practice. Another potential concern is that our likelihood ratio test may preferentially conclude selection in the Native American source if the combined Native American surrogate generally represents a poor match to the true source. Encouragingly, when using PBS to test for selection in LAI-inferred Native American segments from individuals with high degrees of ancestry recently related to the tested Native American source, an analysis that does not use the allele frequency of the combined Native American surrogate, PBS scores for SNPs in 6 of these 18 regions fall into the top 99.99th percentile (supplementary figs. S19–S24, Supplementary Material online), with the remaining 13 regions containing SNPs in the top 99th percentile. However, relative to our approach,

LAI-based selection scans (e.g., [Avila-Arcos et al. \(2020\)](#)) may be more robust to using combined data from multiple populations to represent one surrogate, since it only requires matching to a subset of individuals' haplotype patterns in the reference panel.

We also checked whether the top signals recently reported to be under selection in the Native American ancestry component of an admixed Mexican population using Ohana ([Cheng et al. 2021](#)) showed evidence of selection in our scan of a different Mexican cohort. Notably, we found that 7 out of the top 10 candidate genes reported in [Cheng et al. \(2021\)](#) contained at least one nearby SNP (i.e., within 50 kb from the reported gene) with AdaptMix selection scores above the 95th percentile in the Mexican cohort, including 4 SNPs with scores above the 99th percentile, and one SNP with a score above the 99.9th percentile. We also found that among the 18 SNPs classified as being selected in the Native American ancestors of the Peruvian cohort, 12 of these were found at higher frequencies in ancient DNA (aDNA) from >700-year-old populations sampled in Peru relative to any other aDNA data sampled elsewhere in the Americas ([supplementary fig. S25, Supplementary Material online](#)).

In general, our approach has decreased power to distinguish whether selection occurred post-admixture versus in one of the ancestral sources, if reference population allele frequencies are very different and/or selection is weak ([fig. 1C](#)). Inferring excess ancestry matching using LAI would likely better classify whether selection was post-admixture in such cases, for example, a scenario where one population that is fixed (or nearly fixed) for the protective allele intermixes with a population nearly-fixed for the non-protective allele, with the admixed population subsequently undergoing selection. An example of this is a recently reported excess of African ancestry, likely attributable to post-admixture selection, on the Duffy-null allele in inhabitants of Santiago Island in Cape Verde ([Hamid et al. 2021](#)). However, our test to detect whether *any* type of selection occurred should not be affected by these scenarios. In addition, our approach may identify post-admixture selection in scenarios that excess-ancestry LAI-based would miss by design, such as cases where the selected allele is at a similar frequency in all reference populations. Perhaps the most important contrast to LAI and other approaches detecting selection in admixed populations ([Cheng et al. 2021](#)) is that, in principle, our approach can be applied to populations that descend from the mixture of genetically similar groups, for example, if using haplotype-based approaches (e.g., SOURCEFIND) to infer ancestry proportions. Future work should assess the power of this technique under such admixture settings.

Although our method assumes a single pulse of admixture, theoretically our ability to diagnose and classify selection occurring in only one source should not be affected by multiple instances of (or continuous) admixture from that or any other source. This is because the signal of allele frequency deviation due to selection in such cases is entirely determined by the amount of ancestry inherited from that

source and not by the number of admixture pulses. In contrast, if an admixed population experiences selection and then receives new migrants from one of the original admixing sources that are unaffected by this selection, for example, later European migrants to the Americas, in theory, this may attenuate our ability to determine that selection occurred post-admixture. However, in a simple scenario of one such additional admixture pulse, contributing 10–50% of DNA, the correct post-admixture selection theoretical model fits as well or better to the theoretical truth than does the incorrect model concluding selection in the source that did not contribute new migrants ([supplementary fig. S26, Supplementary Material online](#)).

As noted above, and consistent with other tests comparing populations ([Mathieson 2020](#)), the choice of surrogate group can make a difference in the inferred selection signals. For example, our largest signal of Native American selection, at 10q22 and most strongly signalled in the "Andes Piedmont" Peruvian subgroup, disappears if replacing the "combined Native American" surrogate group with Han Chinese (CHB from the 1KGP) ([supplementary fig. S10, Supplementary Material online](#)). In this case, the frequency of the putatively selected allele (rs5030938) is 67% in LAI-inferred Native American haplotypes in the Peruvian "Andes Piedmont" subgroup, which is notably higher than the 38–54% observed in LAI-inferred Native American haplotypes in four non-Peruvian sub-groups, and, thus, consistent with selection ([supplementary table S7, Supplementary Material online](#)). However, it is lower than that of CHB (~76%), which explains the lack of signal when using CHB as a surrogate. The frequency in Yakut, a Siberian group that perhaps better represents ancestral Native Americans than CHB does ([Wang et al. 2007](#)), is closer to that of frequency estimates across non-Peruvian Native American groups (0.46–0.5). In general, there is a trade-off between using surrogates more distantly related to the source, which may decrease power to find regional adaptation signals, versus choosing a more closely related surrogate, which may also decrease power by masking adaptation signatures that it shares with the target source (e.g., using Iberians as a surrogate for European ancestry of Latin Americans). Our inferred variance parameter can be used to investigate how well a given surrogate captures genetic variation in the target population, with, for example, the inferred variance using CHB as a surrogate ~5–10-fold higher relative to using the combined Native American surrogate.

Selection Signals Detected in the CANDELA Cohort

The candidate genes we infer to be affected by selection in Latin Americans and their Native American ancestors are best viewed in the context of other previously reported signals. [Reynolds et al. \(2019\)](#) recently performed a selection scan in three Native North American populations and identified some of the strongest signals at immune-related genes including the interleukin 1 receptor

Type 1 (*IL1R1*) gene in a sample from several closely related communities in the southeastern United States, and the mucin 19 (*MUC19*) gene in a central Mexican population. We do not replicate the *MUC19* signal in the CANDELA Mexican cohort, which could indicate that the Native American component in this cohort is not closely related to that of the central Mexican Native American group. Nonetheless, we found some of our strongest signals of selection at several loci encompassing genes involved in the immune response, including *CD300LF* and *MIF*, detected as being selected in the Native American ancestors of Peruvians. Interestingly, *CD300LF* promotes macrophage-mediated efferocytosis, whereas *MIF* plays a role regulating macrophage function through the suppression of glucocorticoids. These observations suggest that these two genes might have perhaps evolved in a coordinated manner, possibly due to their phagocytic-related role against the novel pathogens encountered in the Americas.

Regarding signals of selection post-admixture, several studies have consistently shown adaptive signals in different Latin American populations at HLA by showing an excess of matching to African reference haplotypes using LAI (Tang et al. 2007; Basu et al. 2008; Ettinger et al. 2009; Guan 2014; Rishishwar et al. 2015; Deng et al. 2016; Zhou et al. 2016; Norris et al. 2020; Vicuna et al. 2020). Given that African ancestry was enriched at this region, the authors suggested that certain African alleles could have conferred a selective advantage to certain infectious diseases most likely brought by Europeans. Although AdaptMix is only able to classify selection in one cohort (Colombia) out of our four HLA signals, we also replicated this excess of African ancestry in each of the CANDELA cohorts (supplementary fig. S12, Supplementary Material online). There is some debate as to whether these signals are genuine or attributable to confounders such as inaccurate LAI inference (Pasaniuc et al. 2013). To illustrate the validity of these concerns, people with entirely Northwest European ancestry from Britain infer excess ancestry related to Africa in HLA, which—though perhaps influenced by genuine selection at HLA in Northwest Europeans—presumably does not reflect genuine recent African ancestry (supplementary fig. S27, Supplementary Material online). Instead, this is more likely attributable to the relatively high degree of genetic diversity in HLA mimicking African genetic diversity, illustrating how these LAI-based tests can give false-positive signals when testing for post-admixture selection. This may explain why AdaptMix does not replicate the moderate amount of excess African ancestry inferred by LAI at HLA in the Brazilian cohort (supplementary fig. S12, Supplementary Material online), which is predominantly of European ancestry. Indeed, regions under selection in admixed populations may be particularly difficult to classify accurately using LAI, for example, with the HLA region here having the lowest overall LAI classification probability (supplementary fig. S28, Supplementary Material online), especially in cases where the reference population has not experienced similar selection and, hence, may have poorly matching genetic variation patterns. As our approach does not require LAI, it is

robust to these issues. Although our model is not able to classify selection as post-admixture at most of our HLA signals, allele frequency patterns in the admixed cohorts are consistent with post-admixture selection and often show allele frequencies drifting away from those expected under our neutral model and toward those of the African or European reference population (supplementary fig. S29, Supplementary Material online). This is most evident in the Colombian cohort, consistent with Africans contributing protective alleles as previously suggested (Tang et al. 2007; Basu et al. 2008; Ettinger et al. 2009; Guan 2014; Rishishwar et al. 2015; Deng et al. 2016; Zhou et al. 2016; Norris et al. 2020; Vicuna et al. 2020). In addition to HLA, we also identified a novel post-admixture selection signal in the Chilean cohort that was accompanied by a significant increase of European ancestry at the *CD101* locus, again, suggesting that protective alleles from Europeans might have also been adaptive to counter Old World-borne diseases brought to the Americas.

The signals encompassing genes related to metabolic and anthropometric-related phenotypes are consistent with novel dietary practices in the Americas driving adaptation, with many signals with an effect on relevant phenotypes and/or tissues, classified as being selected in the Native American source. Previous studies have shown evidence of adaptation at genes related to metabolic-related phenotypes and attributed the adaptation to dietary pressures in Native Americans. Avila-Arcos et al. (2020) recently reported strong signals of selection in the Mexican Huichol at several genes associated to lipid metabolism, including *APOA5* and *ABCG5*. We do not replicate these signals in the CANDELA Mexican cohort, which could indicate that the Native American component in this cohort is not closely related to that of the Huichol. The signals at *APOA5* and *ABCG5* are in line with a previous finding of a strong selection signal at another ATP-binding cassette transporter A1 (*ABCA1*) gene that has been associated with low high-density lipoprotein cholesterol in Latin Americans (Villarreal-Molina et al. 2008; Acuña-Alonso et al. 2010). As the *ABCA1* protein carrying the putative selected allele shows a decrease cholesterol efflux, the authors suggest that this variant could have favored intracellular cholesterol and energy storage, which, in turn, might have beneficially influenced the ability to accommodate fluctuations in energy supply during severe famines and during the regulation of reproductive function (Acuña-Alonso et al. 2010). Lindo et al. (2018) used a genomic transect of Andean highlanders from northern Peru and found the strongest signals of selection at *MGAM*, a gene related to starch digestion. The authors attributed this finding to a dietary-related selective pressure perhaps brought by the transition to agriculture in this region. AdaptMix shows evidence in the CANDELA Peruvian cohort within *MGAM* ($rs7810984$, AdaptMix P value = 1.79×10^{-8} , above 99.9th percentile) only when using CHB as a surrogate for Native American ancestry. This again illustrates how the choice of surrogate populations defines the selection test between each surrogate and its corresponding ancestral

source. It is possible that by including Andean Native Americans in our Native American source population ([supplementary table S1, Supplementary Material online](#)), we are affecting the power to detect selection in the Andean Native American ancestors of the CANDELA Peruvian cohort, analogous to how [Lindo et al. \(2018\)](#) no longer detect selection at *MGAM* when using PBS to compare ancient and present-day (Aymara) Andean groups.

Studies have also reported signals of selection in Native Americans groups shared with Siberian populations, which the authors interpreted as an adaptation to polyunsaturated-rich diets prior or close to the peopling of the Americas, likely in the Arctic Beringia. These included a signal overlapping the *WARS2* and *TBX15* genes, previously associated to body fat distribution and adipose tissue differentiation ([Fumagalli et al. 2015](#); [Racimo, Gokhman, et al. 2017](#)), and the fatty acid desaturase (FADS) gene cluster that modulates the manufacture of polyunsaturated fatty acids ([Amorim et al. 2017](#); [Harris et al. 2019](#)) (but see [Mathieson \(2020\)](#) for an alternative explanation of the FADS signal). Again, we inferred moderate selection evidence at these regions in the CANDELA Peruvian cohort only when using CHB as surrogate for Native American ancestry (SNP rs2361028 near *TBX15*, AdaptMix *P* value = 1.8×10^{-7} , above 99.5th percentile; SNP rs174576 within *FADS2*, AdaptMix *P* value = 3.8×10^{-8} , above 99.5th percentile). It is, thus, tempting to suggest that the three novel signals of selection AdaptMix classifies as being under selection in Native Americans might be related to dietary pressures experienced prior or during the peopling of the Americas (e.g., the *BRINP3* signal detected in Mexicans), or as a product for a greater reliance of domesticated crops including potatoes (3400–1600 CE) ([Rumold and Aldenderfer 2016](#)) (e.g., the *HKDC1* signal detected in Peruvians). However, it is important to note that other factors may also be attributable to some of these selection signals.

Of potential adaptive interest is the *STOX1* gene detected in the Peruvian cohort close to our highest overall selection signal within *HKDC1* at 10q22 ([fig. 6B](#)). Mutations within *STOX1* have been associated to preeclampsia ([Van Dijk et al. 2005](#); [van Dijk and Oudejans 2011](#)), a pathology of pregnancy characterized by high blood pressure and signs of damage to other organ system that can be lethal for the mother and for the fetus ([Sibai 2003](#)). Interestingly, in a recent linkage study on preeclampsia conducted in Andean Peruvian families, SNPs within *STOX1* show a marginal association (*P* value = 0.004678) ([supplementary fig. S30, Supplementary Material online](#)) ([Badillo Rivera et al. 2021](#)). Given that high elevation is linked to an increased incidence of preeclampsia ([Zamudio 2007](#)), it is possible that natural selection has acted on genes related to this condition. Furthermore, the fact that variants within *HKDC1* are associated with glucose levels in pregnant women ([Hayes et al. 2013](#); [Guo et al. 2015](#); [Kanthimathi et al. 2016](#); [Tan et al. 2019](#)) and considering the relationship between abnormal glucose levels and preeclampsia ([Joffe et al. 1998](#);

[Weissgerber and Mudd 2015](#)), it is also possible that natural selection has targeted variants at *HKDC1* due to its role in glucose metabolism.

Lastly, other environmental factors may also be attributable to some of these selection signals, such as infectious diseases. There is growing evidence of a link between metabolic diseases and innate immunity or inflammation ([Pickup and Crook 1998](#); [Kominsky et al. 2010](#); [Lumeng and Saltiel 2011](#); [Robbins et al. 2014](#)). For instance, it has been shown that cholesterol plays a key role in various infectious processes such as the entry and replication of flaviviral infection ([Osuna-Ramos et al. 2018](#)). Additional studies in ancient and present-day indigenous American populations will be needed to disentangle the putative selective pressures at these loci.

Conclusion

We have presented a novel allele frequency-based method that identifies loci under selection in admixed populations, while determining whether the selection affected all ancestral sources equally, indicating selection following admixture, or in only one of the sources. The novel candidate genes under selection provide new insights into the adaptive traits necessary for the early habitation of the Americas and to respond to the challenge of infectious pathogens corresponding to European contact. Future functional investigations will allow a more detailed understanding of the consequences of selective pressures experienced in the American continent, including its effect on present-day health outcomes.

Materials and Methods

Genomic Datasets

The Latin American individual samples analyzed here were part of the Consortium for the Analysis of the Diversity and Evolution of Latin America (CANDELA) ([Ruiz-Linares et al. 2014](#)). The CANDELA Consortium samples (<http://www.ucl.ac.uk/silva/candela>) have been described in detail in previous publications ([Ruiz-Linares et al. 2014](#); [Chacon-Duque et al. 2018](#)). These data include a total of 6,630 volunteers from five Latin American countries (Brazil, Chile, Colombia, Mexico, and Peru). This dataset was genotyped on the Illumina HumanOmniExpress chip platform including 730,525 SNPs. We also collated reference populations from regions that have contributed to the admixture in Latin America. For Native American samples, we used individuals previously genotyped by [Chacon-Duque et al. \(2018\)](#). This dataset compromises 19 Native American populations from throughout the Americas with genotype data ([supplementary table S1, Supplementary Material online](#)). For all the analyses described, we have only retained Native American individuals that showed more than 99% Native American ancestry as estimated by ADMIXTURE (see below). For European samples, we used genotype data from Portuguese and Spanish,

individuals previously genotyped by Chacon-Duque et al. (2018) and Spanish (IBS; Iberian Population in Spain) from the 1000 Genomes Project study (The 1000 Genomes Project Consortium 2015). For Sub-Saharan Africans, we used genotype data from Yoruba (YRI; Yoruba in Ibadan, Nigeria), and Luhya (LWK; Luhya in Webuye, Kenya) individuals from the 1KGP. The reference samples from Chacon-Duque et al. (2018) are described in more detail in the supplementary table S1 (Supplementary Material online) from the mentioned publication. For some of our analysis, we also included the 103 Han CHB and 85 Europeans from England and Scotland (GBR) from the 1KGP as a surrogate for the Native American and European sources, respectively. Genotype data of the individuals from the 1KGP were downloaded from the 1000 Genomes Project FTP site available at <ftp://ftp.1000genomes.ebi.ac.uk/vol1/ftp/>.

Data Curation

We used PLINK v1.9 (Chang et al. 2015) to exclude SNPs and individuals with more than 5% missing data or that showed evidence of genetic relatedness as in Chacon-Duque et al. (2018). Due to the admixed nature of the Latin American samples, there is an inflation in Hardy–Weinberg *P* values, and, therefore, we did not exclude SNPs based on Hardy–Weinberg deviation. After applying these filters, 625,787 autosomal SNPs and 7,986 individuals were retained for further analysis.

Selecting Admixed Latin American and Reference Individuals

In order to select admixed Latin American individuals (i.e., individuals with varying degrees of Native American, European, and African ancestry), we conducted an unsupervised ADMIXTURE analysis at $K = 3$ using a set of 103,426 LD-pruned SNPs including Native Americans, Iberian Europeans, and West Africans. We then removed nonadmixed Latin American individuals that we define as having less than 10% or more than 90% Native American genome-wide ancestry. To avoid confounding our selection inference due to the underlying population structure, we further excluded individuals with $>1\%$ inferred ancestry matching to surrogates other than Native Americans, Iberian Europeans, and West Africans using SOURCEFIND estimates obtained for the same individuals in Chacon-Duque et al. (2018). As expected, we observe a strong correlation between the ADMIXTURE and SOURCEFIND estimates (average $r > 0.99$), demonstrating the validity of this filtering approach and demonstrating that most of the ancestry of the admixed Latin American individuals can be appropriately modeled by a three-way admixture model. After this filtering procedure, the five Latin American populations consisted of 190 Brazilians (BRA), 1,125 Colombians (COL), 896 Chileans (CHL), 773 Mexicans (MEX), and 834 Peruvians (PER). From our Native American, European, and Sub-Saharan African reference populations, we also removed

individuals who contained more than 1% of ancestry from another group based on the ADMIXTURE analysis described above. After this extra filter, our final reference dataset was composed of 142 Native Americans, 205 Europeans, and 206 Sub-Saharan Africans.

Change in Allele Frequency Under Wright-Fisher with Multiplicative Model of Selection

Assuming a multiplicative model of selection and random mating, the frequency of the three genotypes in generation 1 at a biallelic locus with alleles A and a at frequencies p and $1 - p$, respectively, in the previous generation is where $s_1 \in [-1, \infty]$ is the selection coefficient in generation 1 and

AA	Aa	aa
$(1 + s_1)^2 p^2 / c_1$	$(1 + s_1)2p(1 - p) / c_1$	$(1 - p)^2 / c_1$

$c_1 = (1 + s_1)^2 p^2 + (1 + s_1)2p(1 - p) + (1 - p)^2$. Note that each copy of the A allele changes fitness by a factor of $(1 + s_1)$.

Under the above, the allele frequency of (p_1) of allele A in generation 1 is

$$p_1 = \frac{(1 + s_1)^2 p^2 + (1 + s_1)p(1 - p)}{(1 + s_1)^2 p^2 + (1 + s_1)2p(1 - p) + (1 - p)^2} \quad (1)$$

$$= \frac{(1 + s_1)p}{1 + s_1 p}$$

For generation 2, again assuming a multiplicative selection, the frequencies of the three genotypes are

AA	Aa	aa
$(1 + s_2)^2 p_1^2 / c_2$	$(1 + s_2)2p_1(1 - p_1) / c_2$	$(1 - p_1)^2 / c_2$

where $s_2 \in [-1, \infty]$ is the selection coefficient in generation 2 and $c_2 = (1 + s_2)^2 p_1^2 + (1 + s_2)2p_1(1 - p_1) + (1 - p_1)^2$. Note that each copy of the allele A changes fitness by a factor of $(1 + s_2)$ in this generation.

The allele frequency (p_2) of allele A in generation 2 is

$$p_2 = \frac{(1 + s_2)p_1}{1 + s_2 p_1} \quad (2)$$

$$= \frac{(1 + s_2) \left[\frac{(1 + s_1)p}{1 + s_1 p} \right]}{1 + s_2 \left[\frac{(1 + s_1)p}{1 + s_1 p} \right]} \quad (2)$$

$$= \frac{(1 + s_2^*)p}{1 + s_2^*p},$$

where $s_2^* \equiv (s_1 + s_2 + s_1 s_2)$.

More generally, the allele frequency p_g of allele A in generation g is

$$p_g = \frac{(1 + s^*)p}{1 + s^*p}, \quad (3)$$

where

$$s^* = \left[\sum_{i=1}^g s_i \right] + \left[\sum_{j=1}^{g-1} \left(s_j \sum_{i=j+1}^g s_i \right) \right] + \sum_{i=3}^g \prod_i \approx \sum_{i=1}^g s_i, \quad (4)$$

with s_i the selection coefficient at generation i and \prod_i the sum of the products of all $\binom{g}{i}$ combinations of $\{s_1, \dots, s_i\}$ values. The approximation in equation (4) assumes that the s_i are small, which should be a reasonable approximation based on, for example, the estimated selection coefficients in humans.

Testing for Evidence of Selection at an SNP

To assess the evidence of selection at an SNP, we employ a model inspired by that used in [Mathieson et al. \(2015\)](#) and based on the Balding–Nichols formulation ([Balding and Nichols 1995](#)). In particular, for the allele count X_j at SNP j in the target population, we assume

$$\Pr(X_j = x_j | M, p_j, D) = \text{Beta-Binomial}\left(x_j; 2M, \frac{1-D}{D}p_j, \frac{1-D}{D}(1-p_j)\right), \quad (5)$$

where M is the number of target individuals and D is a variance parameter that is measuring the degree of uncertainty about p_j . More generally, D can be thought of as a genetic drift parameter. The above model implicitly assumes that the frequency of the allele in the target population follows a $\text{Beta}(\text{mean} = p_j, \text{variance} = Dp_j(1-p_j))$. Under neutrality, we assume

$$p_j = \frac{1}{M} \sum_{k=1}^K \left(\left[\sum_{i=1}^M \alpha_k(i) \right] f_{jk} \right), \quad (6)$$

where f_{jk} is the sampled frequency of the allele in the surrogate population at SNP j for source k , and $\alpha_k(i)$ is the inferred admixture proportion from population k in individual i . We first find \hat{D} as the value of D that maximizes $\prod_{j=1}^J [\Pr(X_j | M, p_j, D)]$, using the optim function in R with the “Nelder–Mead” algorithm. Then, fixing $D = \hat{D}$ in equation (5), for each SNP, we find the two-sided P value testing the null hypothesis that the observed allele counts

follow this neutral model.

The variance under (5) is small for SNPs with very high or very low p_j , so such SNPs tend to reject this null model even in cases where the observed target population allele frequency does not deviate notably from its neutral expectation p_j in (6). Therefore, we used an alternative parameterization where we assumed that the frequency of the allele in the target population follows a $\text{Beta}(\text{mean} = p_j, \text{variance} = V)$. This was achieved by substituting D in equation (5) at SNP j with $\min\left[\frac{V}{p_j(1-p_j)}, 0.99999\right]$, necessary to ensure numerical stability, and finding \hat{V} . In practice, this means that SNPs with minor allele frequency $<(1.00001 \times V)$ had variance $(0.99999p_j(1-p_j))$ rather than V . Although our use of V achieved the desired property of mitigating false-positives at SNPs with low MAF, one potential drawback is that datasets containing a high proportion of low-MAF SNPs may drive the inferred V to be small relative to the variance expected at high-MAF SNPs under neutrality. In other words, under neutrality, it is possible that $V > Dp_j(1-p_j)$ at low-MAF SNPs, yet $V < Dp_j(1-p_j)$ at high-MAF SNPs. If so, high-MAF SNPs may reject the neutral model more frequently than it should under neutrality. Indeed, this seems to be the case: in some of our neutral simulations described below, SNPs with *AdaptMix* P value <0.05 are 1.7-fold enriched for SNPs with $\text{MAF} > 0.3$ relative to all tested SNPs. We reiterate that this is partially by design since we use our formulation with V precisely to avoid inferring selection at low-MAF SNPs. Future work, for example inferring V separately for SNPs binned by MAF, may lead to better P value calibration under neutrality.

Determining Whether Selection Occurred Pre or Post-Admixture

Consider the scenario in [figure 1B](#), where sampled population C descends from an admixture of unsampled populations A^* and B^* , who are represented by sampled surrogate populations A and B , respectively. Our test aims to distinguish whether selection occurred post-admixture along branch (e) versus along any of branches (a)–(d). Let f_C be the allele frequency of a sample from population C . At a neutral SNP,

$$E[f_C] = \alpha f_{A^*} + (1 - \alpha) f_{B^*}, \quad (7)$$

where f_{A^*} and f_{B^*} are true allele frequencies of A^* and B^* at the SNP, respectively, and α is the admixture proportion from A^* . Letting f_k be the sampled allele frequency for population k serving as surrogate to the true admixing population k^* , it seems reasonable to assume

$$E[f_C] = \alpha f_A + (1 - \alpha) f_B. \quad (8)$$

Note that this also holds under selection along branch (f) in [figure 1B](#), which we ignore here (but which can be tested by comparing allele frequencies in A and B). Equation (8)

assumes that f_A and f_B are equally good proxies for the admixing populations' frequencies f_A^* and f_B^* , respectively, at the SNP, which may not be true. We test the effect of this using simulations, described below, in which surrogates vary in how well they reflect their respective true admixing sources.

In the case of a multiplicative model of selection along branch (e) in [figure 1B](#) at this SNP, using equation (3), we assume

$$E[f_c] = \frac{(1 + s_c)[\alpha f_A + (1 - \alpha)f_B]}{1 + s_c[\alpha f_A + (1 - \alpha)f_B]} \equiv E_c[f_c], \quad (9)$$

where s_c is the selection strength (i.e., equation (4)) along branch (e).

Alternatively, under a multiplicative model for selection along branches (a) and/or (c) in [figure 1B](#), with analogous results for selection along branches (d) and/or (b), instead we assume

$$\begin{aligned} E[f_c] &= \alpha \left[\frac{(1 + s_A)f_A}{1 + s_A f_A} \right] + (1 - \alpha)f_B \\ &= f_B + \alpha \left[\frac{(1 + s_A)f_A}{1 + s_A f_A} - f_B \right] \equiv E_A[f_c], \end{aligned} \quad (10)$$

where s_A is the selection strength along branches (a) and/or (c). Importantly, $E_A[f_c]$ is linear in α , whereas $E_c[f_c]$ is not, which we aim to exploit to distinguish between these two scenarios.

Here, assuming CANDELA population T can be described as a mixture of K sources, we assume the genotype g_i of individual $i \in [1, \dots, M]$ from T as follows:

$$g_i \sim \text{Binomial}(2, f_T(i)). \quad (11)$$

Under neutrality, we set $f_T(i)$ in equation (11) to

$$f_T^N(i) = \sum_{k=1}^K [\alpha_k(i)f_k], \quad (12)$$

where f_k is the sampled allele frequency at the given SNP for the surrogate population to the source contributing $\alpha_k(i)$ admixture to individual i .

In the case of selection in T post-admixture, we generalize equation (9) and set $f_T(i)$ in equation (11) to

$$f_T^P(i|s) = \frac{(1 + s_c)[\sum_{k=1}^K \alpha_k(i)f_k]}{1 + s_c[\sum_{k=1}^K \alpha_k(i)f_k]}. \quad (13)$$

For the alternative case of selection along the branches separating source A and its sampled surrogate A^* , we generalize equation (10) and replace $f_T(i)$ in equation (11) with

$$f_T^A(i|s_A) = \left[\sum_{k=1}^K \alpha_A(i)f_k \right] + \alpha_A(i) \left[\frac{(1 + s_A)f_A}{1 + s_A f_A} \right]. \quad (14)$$

In practice, we fix $\alpha_k(i)$ to be the proportion of DNA that

each target individual i matches to surrogate k as inferred by ADMIXTURE. We define

$$L^P(s_c) \equiv \prod_{i=1}^M [f_T^P(i|s_c)^{g_i} (1 - f_T^P(i|s_c))^{2-g_i}], \quad (15)$$

where g_i is the genotype for target individual i . We use the optim function in R with the "Nelder–Mead" algorithm to find the maximum-likelihood estimate (MLE) \hat{s}_c , which is the value of s_c that maximizes equation (15).

Similarly, we define

$$L^A(s_A) \equiv \prod_{i=1}^M [f_T^A(i|s_A)^{g_i} (1 - f_T^A(i|s_A))^{2-g_i}], \quad (16)$$

again finding \hat{s}_A as the MLE for s_A .

We note that $[2 - 2\log(L^P(\hat{s}))]$ and $[2 - 2\log(L^A(\hat{s}_A))]$ are analogous to AIC values for these respective models. Following the AIC theory, we calculate

$$I = \frac{\min[L^P(\hat{s}_c), L^A(\hat{s}_A)]}{\max[L^P(\hat{s}_c), L^A(\hat{s}_A)]} \leq 1, \quad (17)$$

where, relative to the model with higher likelihood out of (15) and (16), the model with smaller likelihood is I times as probable to minimize the loss of information when used to represent the unknown true model ([Akaike 1974](#)).

Note we could analogously calculate the likelihood under the neutral model, that is, using equation (12). Then, as an alternative to the selection testing approach described in Section "Testing for evidence of selection at a SNP", we could use a likelihood-ratio-statistic approach to test for selection using either (15) or (16) as the alternative model likelihood. We explored this alternative testing approach but do not use it here because it gave lower P values when simulating under neutrality. This observation may, in part, be alleviated if we estimated f_{k^*} under both the neutral and alternative models rather than fixing $f_{k^*} = f_k$. However, estimating f_{k^*} is confounded with estimating s_c or s_A under the alternative models.

Simulations

Estimating How Well Each Surrogate Reflects its Corresponding True Admixing Source

We aimed to generate simulations that mimic our real data. To do so, we first generate a measure of how well a sampled surrogate population k reflects its corresponding true (unknown) source population. In particular, we estimate a drift parameter d_k in the following manner. First, at each SNP j , we use nlmminb in R to find the estimated values $\{\hat{f}_1^j, \dots, \hat{f}_K^j\}$ for $\{f_1^*, \dots, f_{K^*}\}$, respectively, that minimize

$$\sum_{i=1}^M \left(x_i^j - \sum_{k=1}^K \alpha_k(i)f_{k^*} \right)^2, \quad (18)$$

Table 1. Inferred d_k Measuring How Well the Sampled Surrogate (column) Reflect the True Admixing Sources for Each Target Population (row).

Target	Native American	European	African
Brazil	0.173	0.007	0.102
Chile	0.02	0.011	0.226
Colombia	0.044	0.012	0.044
Mexico	0.024	0.007	0.223
Peru	0.015	0.009	0.119

where $x_i^j \in \{0, 1, 2\}$ is the allele count for the admixed target individual $i \in [1, \dots, M]$ at the SNP and each $\tilde{f}_k^j \in [0, 1]$. Then, for each source k , with observed allele counts G_k^j and total counts M_k^j at SNP j in the surrogate population, following Balding–Nichols (Balding and Nichols 1995) we assume

$$G_k^j \sim \text{Beta} \\ - \text{Binomial}\left(M_k^j, \frac{d_k}{1-d_k} \tilde{f}_k^j, \frac{d_k}{1-d_k} (1-\tilde{f}_k^j)\right). \quad (19)$$

We then used the “Nelder–Mead” algorithm in the optim function in R to find the $d_k \in [0, 1]$ that maximized the product of (19) across all SNPs. This gave the values reported in table 1.

A large estimated $d_k (>0.1)$ corresponds to cases where there is little admixture from that source in our sampled individuals from that country, that is, for African admixture in most countries and Native American admixture in Brazil. As values inferred using such little data are presumably unreliable, we cap them at 0.05 for the simulations below. Although these values are a guide, in practice, we adjusted these values by a multiple of 2–7 to generate neutral simulations that had the same inferred drift \hat{D} , described in section “Testing for evidence of selection at a SNP”, as that observed in the real data.

Generating Simulated Allele Frequencies

We simulated admixed individuals who had experienced selection, with genome-wide admixture proportions $\alpha_k(i)$ from source populations $k \in [1, \dots, K]$ for simulated individuals $i \in [1, \dots, M]$ matching those inferred by ADMIXTURE in the real data. To do so, for each simulation we repeated the following procedure:

- 1) For each source k , at each SNP, we sample starting allele frequencies f_{k*} from a $\text{Beta}\left(\frac{d_k}{1-d_k} f_k, \frac{d_k}{1-d_k} (1-f_k)\right)$, where f_k is the sampled frequency of the respective surrogate population and d_k are defined in table 1 (but capped at 0.05).
- 2) We randomly select SNPs to undergo selection. If selection is occurring in source population k prior to admixture, we randomly sample from among SNPs for which $f_{k*} < 0.5$. If selection is occurring post-

admixture, we instead randomly sample from among SNPs for which $\sum_{i=1}^M \left(\sum_{k=1}^K f_{k*} \alpha_k(i) \right) / M < 0.5$.

- 3) We randomly select neutral SNPs from among all remaining SNPs, that is, those not among the SNPs chosen in (2), in the real data.
- 4) To simulate selection:
 - If selection is occurring prior to admixture, we simulate selection in the relevant source population for g generations under a specified model of selection (additive, dominant, multiplicative, recessive) using Wright–Fisher with a population size of N_e individuals.
 - If selection is occurring after admixture, we simulate selection separately in each of the source populations for g generations, under a specified model of selection using Wright–Fisher with a population size of N_e individuals per population.
- 5) At each SNP, we sample allele counts for each individual i from a $\text{Binomial}(2, p_i)$ with $p_i = \sum_{k=1}^K [f_k^g \alpha_k(i)]$, where
 - $f_k^g = f_{k*}$ for neutral SNPs
 - $f_k^g = f_{k*}$ at selected SNPs for source populations k not undergoing selection (i.e., in cases where selection is pre-admixture)
 - f_k^g is the sampled final frequencies in step (4) after g generations, at selected SNPs for source population k undergoing selection.

We then analyze data from the simulated target population individuals using the real sampled data from the surrogate populations. For simulations here, we use $N_e = 10,000$ for the African, European, and Native American source groups.

Our procedure in steps (4)–(5) to simulate selection and admixture ensures that the admixed individuals have variable admixture proportions while remaining computationally tractable. An alternative to this would be to generate M admixed populations using observed f_k values, with the admixture proportions for population i equal to $\alpha_1(i), \dots, \alpha_K(i)$, and then simulate each admixed population for g generations using Wright–Fisher, either with or without selection. Such simulations would match the approach used by our model to classify selection as type 1 or type 2 (Section “Determining whether selection occurred pre- or post-admixture”). However, we chose the above for reasons of computational efficiency, as we have many individuals (i.e., $M > 1000$). Note also that our selection test (Section “Determining whether selection occurred pre- or post-admixture”) is different from this simulation procedure, in that our test models the combined allele frequency across all admixed individuals, using the mean admixture contributions across target individuals to calculate the expected frequency. This, in addition to the way we infer the variance term that describes the distribution of each SNP’s sampled allele frequency (see “Testing for evidence of selection at a SNP” above), may

explain why our model exhibits an excess of SNPs with small P values even when simulating no selection. This is despite using all SNPs to infer the model's variance parameter, which is designed to make more SNPs fit the model (likely explaining the excess of high P values, we also see, e.g., in [supplementary fig. S17, Supplementary Material](#) online). Although including this variance parameter does somewhat control P values by for example, giving in some cases a median P value near 0.5, as expected under neutrality, our no-selection simulations suggest caution in directly using our model's P values for assessing selection evidence. This suggests that some degree of plausible simulations would be helpful to calibrate the model's reported P values.

Forward Simulations

To explore the effect of the effective population size (N_e) on the population undergoing selection, we conducted additional simulations using the forward simulator SLiM 3 ([Haller and Messer 2019](#)). We used the demographic model of an admixed Mexican (MEX) population recently presented in [Cheng et al. \(2021\)](#). The model is based on parameter estimates from [Gravel et al. \(2011\)](#) and [Gutenkunst et al. \(2009\)](#) of a three-population demography, namely, an African (AFR), European (EUR), and Asian population (ASN). The main difference is the inclusion of an additional Native American population that splits from the ASN population. The MEX population is modeled as a 50%/50% admixture between the EUR and the Native American population. We consider five different N_e s for the Native American population ($N_e = 800, 1,000, 200, 5,000$, and $10,000$). The selection occurs only in the ancestral Native American population with no ongoing selection in MEX. In the original model, selection lasts for 500 generations, which resulted in the allele being fixed before the admixture event in simulations with high N_e , particularly when testing for high selection coefficients. To avoid this fixation which might result in a bias when estimating the power, we modeled selection in the Native American population for 300 generations. All other parameters were the same as in the original model. We simulate a region of 4 Mb with a mutation rate of 10^{-8} and a recombination rate of 10^{-8} base pairs per generation and sample 20 diploid individuals from each population. We simulate a single selected site under an additive model within a ± 10 kb window of the center of the simulated region. As in our previous simulations, we consider 10 different selection coefficients ($s = 0.01$ to 0.1 in steps of 0.01, with s defined here as the increased fitness when carrying one copy of the advantageous allele) with a starting frequency for the selected site being equal to or higher than 0.01 but lower than 0.1. Following [Haller and Messer \(2019\)](#), we scale times down by a factor of 10, and scale up the mutation rate, recombination rate, and selection coefficient by a factor of 10. We conducted a total of 500 independent regions to estimate the statistical power for each combination of N_e and selection coefficient.

We additionally simulated an 80 Mb region under neutrality (i.e., $s = 0$) using the same settings as previously described. For AdaptMix, admixture proportions were estimated by applying supervised ADMIXTURE with $K = 3$ to this neutral region, setting AFR, EUR, and ASN as the reference populations. Note that, as the MEX population does not have AFR ancestry, this simulation setting is also assessing the power under a model misspecification, which might be more realistic for most real-word applications. The 80 Mb neutral region was then used to generate a null distribution of P values. The power of AdaptMix was based on a P value cutoff that resulted in a false-positive rate of 5×10^{-5} of this null distribution.

Comparison of AdaptMix Against Other Selection Approaches

We compared the performance of AdaptMix with two different approaches under the two scenarios: 1) selection in one of the source populations and 2) selection in the admixed population following the admixture event.

To assess the power under scenario 1), we compared AdaptMix against Ohana, a maximum likelihood method for finding regions under positive selection by modeling ancestry components ([Cheng et al. 2021](#)). Importantly, Ohana has been shown to retain similar or higher power compared with other state-of-the-art methods. We compared AdaptMix and Ohana under the demographic setting previously described, but simulating selection for 500 generations and fixing the N_e of the Native American population undergoing selection to 800, as in the original publication.

To assess the power under scenario 2), we compared AdaptMix against Ohana and to a LAD approach. A LAD approach here consists of evaluating whether a genomic region is enriched for a particular ancestry compared with their genome-wide average, and relies on local ancestry inference. LAD approaches have been extensively used to detect signals of selection following an admixture event in several recently admixed populations, including Latin Americans ([Tang et al. 2007; Basu et al. 2008; Ettinger et al. 2009; Guan 2014; Rishishwar et al. 2015; Deng et al. 2016; Zhou et al. 2016; Norris et al. 2020; Vicuna et al. 2020](#)). For this scenario, we used the demographic model recently presented in [Cuadros-Espinoza et al. \(2021\)](#), which involves a simple two-way admixture model. Briefly, the demographic model consists of two populations that split from their common ancestor 2080 generations ago and then intermix 70 generations ago to produce a third admixed population. The admixture proportions are set to 50%/50%, and selection occurs only in the admixed population for 70 generations until the present. All other parameters are set to those presented in the publication, except for the removal of background selection. We sample 50 diploid individuals from each of the three populations, that is, the admixed population and the two intermixing populations X and Y, at the end of the simulation, as in the original publication.

As in our previous simulations, we additionally simulated an 80 Mb region under neutrality (i.e., $s = 0$) using the same settings as previously described for each scenario. In the case of AdaptMix, the 80 Mb neutral region was used to estimate admixture proportions, based on a supervised ADMIXTURE analysis with $K = 2$, using X and Y as surrogates, and to generate a null distribution of P values. In the case of Ohana, we used the 80 Mb neutral region to estimate the ancestral component proportions and the covariance matrix, and to generate a null distribution of log-likelihood ratios from its selection scan. The maximum number of iterations to estimate the ancestral component proportions and the covariance matrix was set to 20. For Ohana, we considered both the global hypothesis testing whether any ancestry component has an outlying score in the covariance matrix, and a population-specific hypothesis testing whether a specific ancestry component has an outlying score. For the population-specific hypothesis, in scenario 1), we tested the ancestry component most representative of the Native American component in MEX, and in scenario 2), we tested the ancestry component most prevalent in the admixed population. In the case of LAD, which was only used for scenario 2), we performed local ancestry inference using both RFMix (Maples et al. 2013) and ELAI (Guan 2014). We ran RFMix with the phase correction feature enabled and performed two rounds of the EM algorithm to improve local ancestry calls. In the case of ELAI, we performed 20 rounds of EM iterations. To obtain local ancestry assignment probabilities, we conducted 10 independent runs and averaged probabilities across all runs, as recommended in the ELAI manual. All other parameters for both methods were set to the default except for the time of admixture, which was set to the true generation time. We performed local ancestry inference on the 80 Mb neutral region to generate a null distribution of Z-scores.

To estimate and compare the power between the different approaches, we simulated a total of 500 independent regions under each scenario and for each selection coefficient tested. Each independent simulation consisted of a 2 Mb region with a mutation rate of 10^{-8} and a recombination rate of 10^{-8} base pairs per generation. We simulate a single selected site under an additive model near the center of the simulated region and consider 5 different selection coefficients ($s = 0.01\text{--}0.05$ in steps of 0.01, with s defined here as the increased fitness when carrying one copy of the advantageous allele). The power of each method was based on a P value cutoff that resulted in a false-positive rate of 0.05 of the respective null distribution.

Finally, we also compared the execution time of AdaptMix and Ohana (supplementary table S8, Supplementary Material online). We find that Ohana was much faster when running on a single node, for example taking 80 s to run on 150 individuals at $>200,000$ SNPs using five iterations, compared with running ADMIXTURE and AdaptMix taking $\sim 5,700$ seconds in the same population.

Estimation of Allele Frequencies in Ancient Native Americans

To estimate allele frequencies in ancient Native Americans, we queried the Allen Ancient DNA Resource (AADR) available at <https://reich.hms.harvard.edu/allen-ancient-dna-resource-aadr-downloadable-genotypes-present-day-and-ancient-dna-data>. We downloaded the “1240K” dataset v50.0, which contains ancient and present-day individuals (from either shotgun sequencing data or in-solution target capture, with a range of coverages) at 1,233,013 sites. In order to obtain data for ancient Native Americans without non-Native American ancestry, we kept only individuals with a reported date of more than 500 years BP from countries in the Americas and the Caribbean that passed the quality control filters as defined in the database. After that, we selected populations with a minimum of 10 non-missing allelic counts when estimating allele frequencies.

Local Ancestry Analysis in the CANDELA Cohort

Local ancestry assignment was conducted using the HMM approach implemented in ELAI (Guan 2014). The phased genotype data needed as input was obtained by using SHAPEIT2 (Delaneau et al. 2012) with default parameter settings. Genetic distances were obtained from the HapMap Phase II genetic map build GRCh37 (Gibbs et al. 2003). As reference continental panels, we used the same Native American, European, and African individuals as in our AdaptMix analysis. ELAI was run setting the admixture generation parameter to 20, and with 20 rounds of EM iterations. To obtain local ancestry assignment probabilities, we conducted 10 independent runs and averaged probabilities across all runs as recommended in the ELAI manual. To test for LAD, we estimated Z-scores for each ancestry across each locus and obtained the corresponding one-sided P values testing for a positive deviation.

Population Branch Statistic (PBS) Analysis in the CANDELA Cohort

We first selected Latin American individuals carrying a specific Native American ancestry component based on the inferred Native American ancestry proportions previously estimated by Chacon-Duque et al 2018 in the CANDELA sample. Specifically, for each Native American ancestry component, we selected CANDELA individuals with $>10\%$ inferred ancestry from that particular Native American ancestry component, and with $<1\%$ combined inferred ancestry, combined across all other Native American components. Thus, each group of admixed Latin Americans was composed primarily of Native American ancestry from a particular Native American component, plus European and African ancestry. We then estimated allele frequencies for each Native American component by considering only alleles (i.e., haplotypes) that were considered of Native American origin with local-ancestry posterior probability >0.9 . We only

computed allele frequencies for a Native American component if all SNPs genome-wide had >100 alleles (haplotypes) assigned to Native American origin. This resulted in allele frequency estimates for six Native American components, including "Quechua", "Andes Piedmont", "Chibcha Paez", "Nahua1", "South Mexico", and "Mapuche" ancestral components (see [Chacon-Duque et al. \(2018\)](#) for a detailed description of the inferred components). Pairwise, F_{ST} were then estimated using Hudson's estimator as in equation (9) of [Bhatia et al. \(2013\)](#). The branch length (T) between two populations was computed as $T = -\log_{10}(1 - F_{ST})$ ([Cavalli-Sforza 1969](#)). The Population Branch Statistic (PBS) ([Yi et al. 2010](#)) combines the pairwise branch lengths between three populations, which was computed as

$$PBS_{Target} = \frac{T^{Target,Control} + T^{Target,Outgroup} + T^{Control,Outgroup}}{2}.$$

PBS values were computed for each Native American component, using all possible pairwise combinations of the other Native components as the control and outgroup populations. The rationale of this analysis was to try to find signals of selection exclusive to a given Native American group (i.e., that likely occurred after the divergence between Native American lineages). For some of our analysis, we also used the CHB population from the 1000 Genomes Project, the European reference population, or the African reference population, as control and outgroup populations.

Summary Statistics for GWAS and eQTL Data

To assess the biological consequence of selected variants, we queried summary statistics from genome-wide association studies (GWASs) of relevant phenotypes, and gene-expression data (i.e. expression quantitative locus [eQTL] studies) from relevant cell or tissues. For our GWAS query, we retrieved data from immune and metabolic-related phenotypes, as these traits are known to have been subjected to strong selective pressures across several human groups ([Fan et al. 2016](#)). Immune-related phenotypes included 1) total white cell count, neutrophil count, lymphocyte count, monocyte count, basophil count, and eosinophil count from the [Chen et al. \(2020\)](#) GWAS study conducted across five continental ancestry groups. Metabolic-related phenotypes included the body mass index (BMI), body fat percentage, type II diabetes status, hip circumference, waist circumference, HDL levels, LDL levels, cholesterol levels, and triglyceride levels ([Loh et al. 2018](#)). Summary statistics from these GWAS analyses were based on the UK Biobank (UKBB) cohort available at: <http://www.nealelab.is/uk-biobank>. For our eQTL query, we retrieved the cis-associations summary statistics of 15 human immune cell types from the DICE (Database of Immune Cell Expression, Expression quantitative trait loci [eQTLs] and Epigenomics) project ([Schmiedel et al. 2018](#)), available at: <https://dice-database.org/downloads>. We also retrieved cis-association summary statistics from adipose (subcutaneous, and visceral omentum), muscle

(skeletal), and liver tissue from the GTEx Project v7 ([Lonsdale et al. 2013](#)) available at: <https://gtexportal.org/home/datasets>.

Supplementary Material

[Supplementary data](#) are available at *Molecular Biology and Evolution* online.

Acknowledgments

We thank the volunteers for their enthusiastic support for this research. We also thank Alvaro Alvarado, Mónica Ballesteros Romero, Ricardo Cebrecos, Miguel Ángel Contreras Sieck, Francisco de Ávila Becerril, Joyce De la Piedra, María Teresa Del Solar, Paola Everardo Martínez, William Flores, Martha Granados Riveros, Rosilene Paim, Ricardo Gunski, Sergeant João Felisberto Menezes Cavalheiro, Major Eugênio Correa de Souza Junior, Wendy Hart, Ilich Jafet Moreno, Paola León-Mimila, Francisco Quispealaya, Diana Rogel Diaz, Ruth Rojas, and Vanessa Sarabia, for assistance with volunteer recruitment, sample processing, and data entry. We also thank Francois Balloux, Aida Andres, Mark McCarthy, Etienne Patin, and Sebastian Cuadros Espinoza for helpful discussion and critical comments on earlier versions of the manuscript. We are very grateful to the institutions that allowed the use of their facilities for the assessment of volunteers, including Escuela Nacional de Antropología e Historia and Universidad Nacional Autónoma de México (México); Universidade Federal do Rio Grande do Sul (Brazil); 13º Companhia de Comunicações Mecanizada do Exército Brasileiro (Brazil); Pontifícia Universidad Católica del Perú, Universidad de Lima and Universidad Nacional Mayor de San Marcos (Perú). Work leading to this publication received funds from the following: the Leverhulme Trust (RPG-2018-208 to MF), the National Natural Science Foundation of China (#31771393 to ARL), the Scientific and Technology Committee of Shanghai Municipality (18490750300 to ARL), the Ministry of Science and Technology of China (2020YFE0201600 to ARL), the Shanghai Municipal Science and Technology Major Project (2017SHZDZX01 to ARL) and the 111 Project (B13016 to ARL), the Leverhulme Trust (F/07 134/DF to ARL), BBSRC (BB/I021213/1 to ARL), the Excellence Initiative of Aix-Marseille University - A*MIDEX (a French "Investissements d'Avenir" programme to ARL), Wellcome Trust/Royal Society (098386/Z/12/Z to GH), the National Institute for Health Research University College London Hospitals Biomedical Research Centre, BBSRC (BB/R01356X/1), Universidad de Antioquia (CODI sostenibilidad de grupos 2013- 2014 and MASO 2013-2014), Conselho Nacional de Desenvolvimento Científico e Tecnológico, Fundação de Amparo à Pesquisa do Estado do Rio Grande do Sul (Apoio a Núcleos de Excelência Program), and Fundação de Aperfeiçoamento de Pessoal de Nível Superior. JM-R

was supported by a doctoral scholarship from CONCYTEC-PERU (224-2014-FONDECYT).

Data Availability

This project analyzes only data that have been previously reported in other publications. Raw genotype data for reference populations can be accessed as described previously (The 1000 Genomes Project Consortium 2015; Chacon-Duque et al. 2018). Raw genotype data from CANDELA cannot be made available due to restrictions imposed by ethical approval. Summary statistics from the selection analysis will be deposited in a public repository upon publication.

Software Availability

Scripts for selection analyses will be uploaded to a software developer public repository upon publication. The current version of AdaptMix presented in this study is available upon request from g.hellenthal@ucl.ac.uk.

References

Cavalli-Sforza LL editor.; 1969.

The 1000 Genomes Project Consortium. 2015. A global reference for human genetic variation. *Nature* **526**:68–74.

Acuña-Alonso V, Flores-Dorantes T, Kruit JK, Villarreal-Molina T, Arellano-Campos O, Hünemeier T, Moreno-Estrada A, Ortiz-López MG, Villamil-Ramírez H, León-Mimila P, et al. 2010. A functional ABCA1 gene variant is associated with low HDL-cholesterol levels and shows evidence of positive selection in Native Americans. *Hum Mol Genet*. **19**:2877–2885.

Akaike H. 1974. A new look at the statistical model identification. *IEEE Trans Automatic Control* **19**:716–723.

Alexander DH, Novembre J, Lange K. 2009. Fast model-based estimation of ancestry in unrelated individuals. *Genome Res*. **19**:1655–1664.

Amorim CE, Nunes K, Meyer D, Comas D, Bortolini MC, Salzano FM, Hunemeier T. 2017. Genetic signature of natural selection in first Americans. *Proc Natl Acad Sci U S A*. **114**:2195–2199.

Avila-Arcos MC, McManus KF, Sandoval K, Rodriguez-Rodriguez JE, Villa-Islas V, Martin AR, Luisi P, Penalosa-Espinosa RI, Eng C, Huntsman S, et al. 2020. Population history and gene divergence in Native Mexicans inferred from 76 human exomes. *Mol Biol Evol*. **37**:994–1006.

Badillo Rivera KM, Nieves-Colon MA, Mendoza KS, Davalos VV, Lencinas LEE, Chen JW, Zhang ET, Sockell A, Tello PO, Hurtado GM, et al. 2021. Clotting factor genes are associated with pre-eclampsia in high altitude pregnant women in the Peruvian Andes. *medRxiv*.

Balding DJ, Nichols RA. 1995. A method for quantifying differentiation between populations at multi-allelic loci and its implications for investigating identity and paternity. *Genetica* **96**:3–12.

Basu A, Tang H, Zhu X, Gu CC, Hanis C, Boerwinkle E, Risch N. 2008. Genome-wide distribution of ancestry in Mexican Americans. *Hum Genet*. **124**:207–214.

Bersaglieri T, Sabeti PC, Patterson N, Vanderploeg T, Schaffner SF, Drake JA, Rhodes M, Reich DE, Hirschhorn JN. 2004. Genetic signatures of strong recent positive selection at the lactase gene. *Am J Hum Genet*. **74**:1111–1120.

Bhatia G, Patterson N, Sankararaman S, Price AL. 2013. Estimating and interpreting FST: the impact of rare variants. *Genome Res*. **23**:1514–1521.

Bhatia G, Tandon A, Patterson N, Aldrich MC, Ambrosone CB, Amos C, Bandera EV, Berndt SI, Bernstein L, Blot WJ, et al. 2014. Genome-wide scan of 29,141 African Americans finds no evidence of directional selection since admixture. *Am J Hum Genet*. **95**:437–444.

Borrego F. 2013. The CD300 molecules: an emerging family of regulators of the immune system. *Blood* **121**:1951–1960.

Bouloc A, Bagot M, Delaire S, Bensussan A, Boumsell L. 2000. Triggering CD101 molecule on human cutaneous dendritic cells inhibits T cell proliferation via IL-10 production. *Eur J Immunol*. **30**:3132–3139.

Calandra T, Roger T. 2003. Macrophage migration inhibitory factor: a regulator of innate immunity. *Nat Rev Immunol*. **3**:791–800.

Chacon-Duque JC, Adhikari K, Fuentes-Guajardo M, Mendoza-Revilla J, Acuña-Alonso V, Barquera R, Quinto-Sánchez M, Gomez-Valdes J, Everardo Martinez P, Villamil-Ramírez H, et al. 2018. Latin Americans show widespread Converso ancestry and imprint of local Native ancestry on physical appearance. *Nat Commun*. **9**:5388.

Chang CC, Chow CC, Tellier LC, Vattikuti S, Purcell SM, Lee JJ. 2015. Second-generation PLINK: rising to the challenge of larger and richer datasets. *Gigascience* **4**:7.

Chen M-H, Raffield LM, Mousas A, Sakaue S, Huffman JE, Moscati A, Trivedi B, Jiang T, Akbari P, Vuckovic D, et al. 2020. Trans-ethnic and ancestry-specific blood-cell genetics in 746,667 individuals from 5 global populations. *Cell* **182**:1198–1213.e14.

Cheng JY, Stern AJ, Racimo F, Nielsen R. 2021. Detecting selection in multiple populations by modelling ancestral admixture components. *Mol Biol Evol*. **9**:msab294.

Cuadros-Espinoza S, Laval G, Quintana-Murci L, Patin E. 2021. The genomic signatures of natural selection in admixed human populations. *bioRxiv*.

Delaneau O, Marchini J, Zagury J-F. 2012. A linear complexity phasing method for thousands of genomes. *Nat Methods* **9**:179–181.

Deng L, Ruiz-Linares A, Xu S, Wang S. 2016. Ancestry variation and footprints of natural selection along the genome in Latin American populations. *Sci Rep*. **6**:21766.

Ettinger NA, Duggal P, Braz RF, Nascimento ET, Beaty TH, Jeronimo SM, Pearson RD, Blackwell JM, Moreno L, Wilson ME. 2009. Genetic admixture in Brazilians exposed to infection with *Leishmania chagasi*. *Ann Hum Genet*. **73**:304–313.

Fan S, Hansen ME, Lo Y, Tishkoff SA. 2016. Going global by adapting local: a review of recent human adaptation. *Science* **354**:54–59.

Fumagalli M, Moltke I, Grarup N, Racimo F, Bjerregaard P, Jørgensen ME, Korneliussen TS, Gerbault P, Skotte L, Linneberg A. 2015. Greenlandic Inuit show genetic signatures of diet and climate adaptation. *Science* **349**:1343–1347.

Galinsky KJ, Bhatia G, Loh PR, Georgiev S, Mukherjee S, Patterson NJ, Price AL. 2016. Fast principal-component analysis reveals convergent evolution of ADH1B in Europe and East Asia. *The American Journal of Human Genetics* **98**:456–472.

Ghoussaini M, Mountjoy E, Carmona M, Peat G, Schmidt EM, Hercules A, Fumis L, Miranda A, Carvalho-Silva D, Buniello A. 2021. Open Targets Genetics: systematic identification of trait-associated genes using large-scale genetics and functional genomics. *Nucl Acids Res*. **49**:D1311–D1320.

Gibbs RA, Belmont JW, Hardenbol P, Willis TD, Yu F, Yang H, Ch'ang L-Y, Huang W, Liu B, Shen Y. 2003. The international HapMap project.

Giri A, Hellwege JN, Keaton JM, Park J, Qiu C, Warren HR, Torstenson ES, Kovesdy CP, Sun YV, Wilson OD. 2019. Trans-ethnic association study of blood pressure determinants in over 750,000 individuals. *Nat Genet*. **51**:51–62.

Gravel S, Henn BM, Gutenkunst RN, Indap AR, Marth GT, Clark AG, Yu F, Gibbs RA, Bustamante CD, 1000 Genomes Project. 2011. Demographic history and rare allele sharing among human populations. *Proc Natl Acad Sci U S A*. **108**:11983–11988.

Gu S, Li H, Pakstis AJ, Speed WC, Gurwitz D, Kidd JR, Kidd KK. 2018. Recent selection on a class I ADH locus distinguishes Southwest Asian populations including Ashkenazi Jews. *Genes (Basel)* **9**:452.

Guan Y. 2014. Detecting structure of haplotypes and local ancestry. *Genetics* **196**:625–642.

Guo C, Ludvik AE, Arlotto ME, Hayes MG, Armstrong LL, Scholtens DM, Brown CD, Newgard CB, Becker TC, Layden BT, et al. 2015. Coordinated regulatory variation associated with gestational hyperglycaemia regulates expression of the novel hexokinase HKDC1. *Nat Commun.* **6**:1–8.

Gutenkunst RN, Hernandez RD, Williamson SH, Bustamante CD. 2009. Inferring the joint demographic history of multiple populations from multidimensional SNP frequency data. *PLoS Genet.* **5**:e1000695.

Haak W, Lazaridis I, Patterson N, Rohland N, Mallick S, Llamas B, Brandt G, Nordenfelt S, Harney E, Stewardson K, et al. 2015. Massive migration from the steppe was a source for Indo-European languages in Europe. *Nature* **522**:207–211.

Haller BC, Messer PW. 2019. SLiM 3: forward genetic simulations beyond the Wright–Fisher model. *Mol Biol Evol.* **36**:632–637.

Hamid I, Korunes KL, Beleza S, Goldberg A. 2021. Rapid adaptation to malaria facilitated by admixture in the human population of Cabo Verde. *Elife* **10**:e63177.

Hancock AM, Witonsky DB, Ehler E, Alkorta-Aranburu G, Beall C, Gebremedhin A, Sukernik R, Utermann G, Pritchard J, Coop G, et al. 2010. Human adaptations to diet, subsistence, and environment are due to subtle shifts in allele frequency. *Proc Natl Acad Sci U S A.* **107**:8924–8930.

Harris DN, Ruczinski I, Yanek LR, Becker LC, Becker DM, Guio H, Cui T, Chilton FH, Mathias RA, O'Connor TD. 2019. Evolution of hominin polyunsaturated fatty acid metabolism: from Africa to the New World. *Genome Biol Evol.* **11**:1417–1430.

Hayes MG, Urbanek M, Hivert M-F, Armstrong LL, Morrison J, Guo C, Lowe LP, Scheftner DA, Pluzhnikov A, Levine DM, et al. 2013. Identification of HKDC1 and BACE2 as genes influencing glycemic traits during pregnancy through genome-wide association studies. *Diabetes* **62**:3282–3291.

Hellenthal G, Busby GBJ, Band G, Wilson JF, Capelli C, Falush D, Myers S. 2014. A genetic atlas of human admixture history. *Science* **343**:747–751.

Hodgson JA, Pickrell JK, Pearson LN, Quillen EE, Prista A, Rocha J, Soodyall H, Shriver MD, Perry GH. 2014. Natural selection for the Duffy-null allele in the recently admixed people of Madagascar. *Proc Biol Sci.* **281**:20140930.

Hoffmann TJ, Ehret GB, Nandakumar P, Ranatunga D, Schaefer C, Kwok P-Y, Iribarren C, Chakravarti A, Risch N. 2017. Genome-wide association analyses using electronic health records identify new loci influencing blood pressure variation. *Nat Genet.* **49**:54–64.

Homburger JR, Moreno-Estrada A, Gignoux CR, Nelson D, Sanchez E, Ortiz-Tello P, Pons-Estel BA, Acevedo-Vasquez E, Miranda P, Langefeld CD, et al. 2015. Genomic insights into the ancestry and demographic history of South America. *PLoS Genet.* **11**:e1005602.

Joffe GM, Esterlitz JR, Levine RJ, Clemens JD, Ewell MG, Sibai BM, Catalano PM. 1998. The relationship between abnormal glucose tolerance and hypertensive disorders of pregnancy in healthy nulliparous women. *Am J Obstet Gynecol.* **179**:1032–1037.

Kanthimathi S, Liju S, Laasya D, Anjana RM, Mohan V, Radha V. 2016. Hexokinase domain containing 1 (HKDC1) gene variants and their association with gestational diabetes mellitus in a south Indian population. *Ann Hum Genet.* **80**:241–245.

Karlsson EK, Kwiatkowski DP, Sabeti PC. 2014. Natural selection and infectious disease in human populations. *Nat Rev Genet.* **15**:379–393.

Kominsky DJ, Campbell EL, Colgan SP. 2010. Metabolic shifts in immunity and inflammation. *J Immunol.* **184**:4062–4068.

Koscielny G, An P, Carvalho-Silva D, Cham JA, Fumis L, Gasparyan R, Hasan S, Karamanis N, Maguire M, Papa E, et al. 2017. Open targets: a platform for therapeutic target identification and validation. *Nucl Acids Res.* **45**:D985–D994.

Lazaridis I, Patterson N, Mittnik A, Renaud G, Mallick S, Kirsanow K, Sudmant PH, Schraiber JG, Castellano S, Lipson M, et al. 2014. Ancient human genomes suggest three ancestral populations for present-day Europeans. *Nature* **513**:409–413.

Lindo J, Haas R, Hofman C, Apata M, Moraga M, Verdugo RA, Watson JT, Llave CV, Witonsky D, Beall C, et al. 2018. The genetic prehistory of the Andean highlands 7000 years BP through European contact. *Sci Adv.* **4**:eaau4921.

Loh PR, Kichaev G, Gazal S, Schoech AP, Price AL. 2018. Mixed-model association for biobank-scale datasets. *Nat Genet.* **50**:906–908.

Long JC. 1991. The genetic structure of admixed populations. *Genetics* **127**:417–428.

Lonsdale J, Thomas J, Salvatore M, Phillips R, Lo E, Shad S, Hasz R, Walters G, Garcia F, Young N, et al. 2013. The genotype-tissue expression (GTEx) project. *Nat Genet.* **45**:580–585.

Ludvik AE, Pusec CM, Priyadarshini M, Angueira AR, Guo C, Lo A, Hershenhouse KS, Yang G-Y, Ding X, Reddy TE, et al. 2016. HKDC1 is a novel hexokinase involved in whole-body glucose use. *Endocrinology* **157**:3452–3461.

Luisi P, García A, Berros JM, Motti JM, Demarchi DA, Alfaro E, Aquilano E, Argüelles C, Avena S, Bailliet G, et al. 2020. Fine-scale genomic analyses of admixed individuals reveal unrecognized genetic ancestry components in Argentina. *PLoS one* **15**:e0233808.

Lumeng CN, Saltiel AR. 2011. Inflammatory links between obesity and metabolic disease. *J Clin Invest.* **121**:2111–2117.

Maples BK, Gravel S, Kenny EE, Bustamante CD. 2013. RFMix: a discriminative modeling approach for rapid and robust local-ancestry inference. *Am J Hum Genet.* **93**:278–288.

Mathieson I. 2020. Limited evidence for selection at the FADS locus in Native American populations. *Mol Biol. Evol.* **37**:2029–2033.

Mathieson I, Lazaridis I, Rohland N, Mallick S, Patterson N, Rozenberg SA, Harney E, Stewardson K, Fernandes D, Novak M, et al. 2015. Genome-wide patterns of selection in 230 ancient Eurasians. *Nature* **528**:499–503.

Moreno-Estrada A, Gignoux CR, Fernandez-Lopez JC, Zakharia F, Sikora M, Contreras AV, Acuna-Alonso V, Sandoval K, Eng C, Romero-Hidalgo S, et al. 2014. Human genetics. The genetics of Mexico recapitulates Native American substructure and affects biomedical traits. *Science* **344**:1280–1285.

Moreno-Estrada A, Gravel S, Zakharia F, McCauley JL, Byrnes JK, Gignoux CR, Ortiz-Tello PA, Martinez RJ, Hedges DJ, Morris RW, et al. 2013. Reconstructing the population genetic history of the Caribbean. *PLoS Genet.* **9**:e1003925.

Norris ET, Rishishwar L, Chande AT, Conley AB, Ye K, Valderrama-Aguirre A, Jordan IK. 2020. Admixture-enabled selection for rapid adaptive evolution in the Americas. *Genome Biol.* **21**:29.

Ochoa D, Hercules A, Carmona M, Suveges D, Gonzalez-Uriarte A, Malangone C, Miranda A, Fumis L, Carvalho-Silva D, Spitzer M, et al. 2021. Open Targets Platform: supporting systematic drug–target identification and prioritisation. *Nucl Acids Res.* **49**:D1302–D1310.

Osuna-Ramos JF, Reyes-Ruiz JM, Del Ángel RM. 2018. The role of host cholesterol during flavivirus infection. *Front Cell Infect Microbiol.* **8**:388.

Pasaniuc B, Sankararaman S, Torgerson DG, Gignoux C, Zaitlen N, Eng C, Rodriguez-Cintron W, Chapela R, Ford JG, Avila PC, et al. 2013. Analysis of Latino populations from GALA and MEC studies reveals genomic loci with biased local ancestry estimation. *Bioinformatics* **29**:1407–1415.

Patterson N, Moorjani P, Luo Y, Mallick S, Rohland N, Zhan Y, Genschoreck T, Webster T, Reich D. 2012. Ancient admixture in human history. *Genetics* **192**:1065–1093.

Pickup J, Crook M. 1998. Is type II diabetes mellitus a disease of the innate immune system? *Diabetologia* **41**:1241–1248.

Pierron D, Heiske M, Razafindrazaka H, Pereda-Loth V, Sanchez J, Alva O, Arachiche A, Boland A, Olaso R, Deleuze JF, et al. 2018. Strong selection during the last millennium for African ancestry in the admixed population of Madagascar. *Nat Commun.* **9**:932.

Poulter M, Hollox E, Harvey CB, Mulcare C, Peuhkuri K, Kajander K, Sarner M, Korpela R, Swallow DM. 2003. The causal element for the lactase persistence/non-persistence polymorphism is located in a 1 Mb region of linkage disequilibrium in Europeans. *Ann Hum Genet.* **67**:298–311.

Pulit SL, Stoneman C, Morris AP, Wood AR, Glastonbury CA, Tyrrell J, Yengo L, Ferreira T, Marouli E, Ji Y, et al. 2019. Meta-analysis of genome-wide association studies for body fat distribution in 694 649 individuals of European ancestry. *Hum Mol Genet* **28**:166–174.

Racimo F, Gokhman D, Fumagalli M, Ko A, Hansen T, Moltke I, Albrechtsen A, Carmel L, Huerta-Sánchez E, Nielsen R. 2017. Archaic adaptive introgression in TBX15/WARS2. *Mol Biol Evol.* **34**:509–524.

Racimo F, Marnetto D, Huerta-Sánchez E. 2017. Signatures of archaic adaptive introgression in present-day human populations. *Mol Biol Evol.* **34**:296–317.

Refoyo-Martínez A, da Fonseca RR, Halldórsdóttir K, Árnason E, Mailund T, Racimo F. 2019. Identifying loci under positive selection in complex population histories. *Genome Res.* **29**: 1506–1520.

Reynolds AW, Mata-Miguez J, Miro-Herrans A, Briggs-Cloud M, Sylestine A, Barajas-Olmos F, Garcia-Ortiz H, Rzhetskaya M, Orozco L, Raff JA, et al. 2019. Comparing signals of natural selection between three Indigenous North American populations. *Proc Natl Acad Sci U S A.* **116**:9312–9317.

Rishishwar L, Conley AB, Wigington CH, Wang L, Valderrama-Aguirre A, Jordan IK. 2015. Ancestry, admixture and fitness in Colombian genomes. *Sci Rep.* **5**:12376.

Robbins GR, Wen H, Ting JP-Y. 2014. Inflammasomes and metabolic disorders: old genes in modern diseases. *Mol Cell* **54**:297–308.

Ruiz-Linares A, Adhikari K, Acuna-Alonso V, Quinto-Sánchez M, Jaramillo C, Arias W, Fuentes M, Pizarro M, Everardo P, de Avila F, et al. 2014. Admixture in Latin America: geographic structure, phenotypic diversity and self-perception of ancestry based on 7,342 individuals. *PLoS Genet.* **10**:e1004572.

Rumold CU, Aldenderfer MS. 2016. Late Archaic–Early Formative period microbotanical evidence for potato at Jiskairumoko in the Titicaca Basin of southern Peru. *Proc Natl Acad Sci U S A.* **113**:13672–13677.

Santoscoy-Ascencio G, Baños-Hernández CJ, Navarro-Zarza JE, Hernández-Bello J, Bucala R, López-Quintero A, Valdés-Alvarado E, Parra-Rojas I, Illades-Aguiar B, Muñoz-Valle JF. 2020. Macrophage migration inhibitory factor promoter polymorphisms are associated with disease activity in rheumatoid arthritis patients from Southern Mexico. *Mol Genet Genomic Med.* **8**:e1037.

Schmiedel BJ, Singh D, Madrigal A, Valdovino-Gonzalez AG, White BM, Zapardiel-Gonzalo J, Ha B, Altay G, Greenbaum JA, McVicker G, et al. 2018. Impact of genetic polymorphisms on human immune cell gene expression. *Cell* **175**:1701–1715.e16.

Shuai K, Liu B. 2003. Regulation of JAK–STAT signalling in the immune system. *Nat Rev Immunol.* **3**:900–911.

Sibai BM. 2003. Diagnosis and management of gestational hypertension and preeclampsia. *Obstet Gynecol.* **102**:181–192.

Sirugo G, Williams SM, Tishkoff SA. 2019. The missing diversity in human genetic studies. *Cell* **177**:1080.

Soares LR, Tsavaler L, Rivas A, Engleman EG. 1998. V7 (CD101) ligation inhibits TCR/CD3-induced IL-2 production by blocking Ca²⁺ flux and nuclear factor of activated T cell nuclear translocation. *J Immunol.* **161**:209–217.

Tan Y-X, Hu S-M, You Y-P, Yang G-L, Wang W. 2019. Replication of previous genome-wide association studies of HKDC1, BACE2, SLC16A11 and TMEM163 SNPs in a gestational diabetes mellitus case–control sample from Han Chinese population. *Diabetes Metab Syndr Obes: Targets Therapy* **12**:983–989.

Tang H, Choudhry S, Mei R, Morgan M, Rodriguez-Cintron W, Burchard EG, Risch NJ. 2007. Recent genetic selection in the ancestral admixture of Puerto Ricans. *Am J Hum Genet.* **81**: 626–633.

Van Dijk M, Mulders J, Poutsma A, Könst AA, Lachmeijer AM, Dekker GA, Blankenstein MA, Oudejans CB. 2005. Maternal segregation of the Dutch preeclampsia locus at 10q22 with a new member of the winged helix gene family. *Nat Genet.* **37**:514–519.

van Dijk M, Oudejans C. 2011. STOX1: key player in trophoblast dysfunction underlying early onset preeclampsia with growth retardation. *J Pregnancy* **2011**:521826.

Vicente M, Priejhodova E, Diallo I, Podgorna E, Poloni ES, Cerny V, Schlebusch CM. 2019. Population history and genetic adaptation of the Fulani nomads: inferences from genome-wide data and the lactase persistence trait. *BMC Genomics* **20**:915.

Vicuna L, Klimenkova O, Norambuena T, Martinez FI, Fernandez MI, Shchur V, Eyheramendy S. 2020. Postadmixture selection on Chileans targets haplotype involved in pigmentation, thermogenesis and immune defense against pathogens. *Genome Biol Evol.* **12**:1459–1470.

Villarreal-Molina MT, Flores-Dorantes MT, Arellano-Campos O, Villalobos-Companan M, Rodríguez-Cruz M, Miliar-García A, Huertas-Vazquez A, Menjivar M, Romero-Hidalgo S, Wacher NH, et al. 2008. Association of the ATP-binding cassette transporter A1 R230C variant with early-onset type 2 diabetes in a Mexican population. *Diabetes* **57**:509–513.

Wang S, Lewis CM, Jakobsson M, Ramachandran S, Ray N, Bedoya G, Rojas W, Parra MV, Molina JA, Gallo C, et al. 2007. Genetic variation and population structure in native Americans. *PLoS Genet.* **3**:e185.

Warren HR, Evangelou E, Cabrera CP, Gao H, Ren M, Mifsud B, Ntalla I, Surendran P, Liu C, Cook JP. 2017. Genome-wide association analysis identifies novel blood pressure loci and offers biological insights into cardiovascular risk. *Nat Genet.* **49**:403–415.

Warrington NM, Beaumont RN, Horikoshi M, Day FR, Helgeland Ø, Laurin C, Bacelis J, Peng S, Hao K, Feenstra B, et al. 2019. Maternal and fetal genetic effects on birth weight and their relevance to cardio-metabolic risk factors. *Nat Genet.* **51**:804–814.

Weissgerber TL, Mudd LM. 2015. Preeclampsia and diabetes. *Curr Diab Rep.* **15**:1–10.

Yi X, Liang Y, Huerta-Sánchez E, Jin X, Cuo ZXP, Pool JE, Xu X, Jiang H, Vinckenbosch N, Korneliussen TS, et al. 2010. Sequencing of 50 human exomes reveals adaptation to high altitude. *Science* **329**:75–78.

Zamudio S. 2007. High-altitude hypoxia and preeclampsia. *Front Biosci.* **12**:2967.

Zhou Q, Zhao L, Guan Y. 2016. Strong selection at MHC in Mexicans since admixture. *PLoS Genet.* **12**:e1005847.

Zhu Z, Guo Y, Shi H, Liu C-L, Panganiban RA, Chung W, O'Connor LJ, Himes BE, Gazal S, Hasegawa K. 2020. Shared genetic and experimental links between obesity-related traits and asthma subtypes in UK Biobank. *J Allergy Clin Immunol.* **145**:537–549.